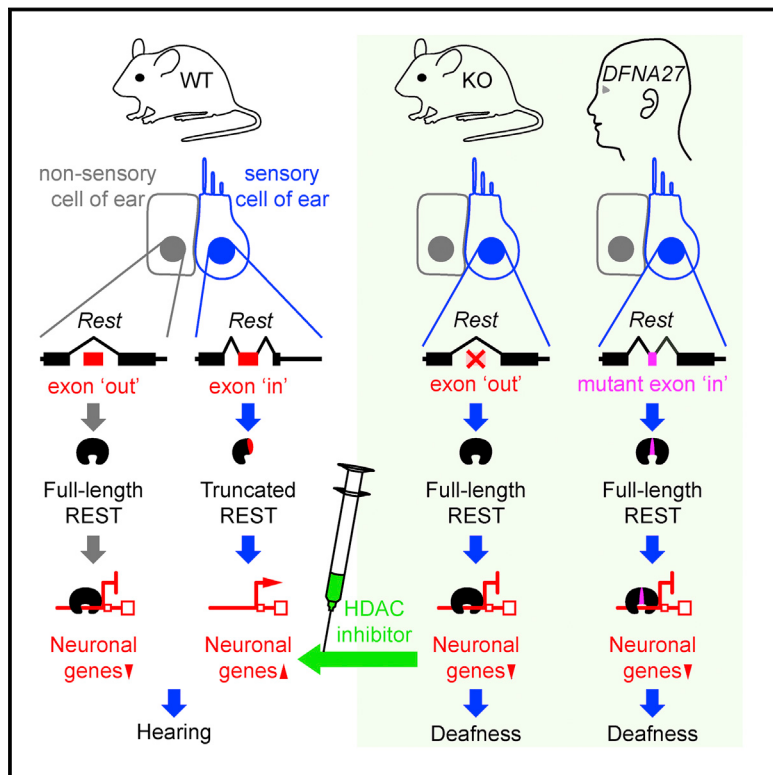


Defects in the Alternative Splicing-Dependent Regulation of REST Cause Deafness

Graphical Abstract



Authors

Yoko Nakano, Michael C. Kelly,
Atteeq U. Rehman, ..., Matthew W. Kelley,
Thomas B. Friedman, Botond Bánfi

Correspondence

botond-banfi@uiowa.edu

In Brief

A *REST* mutation impacting its alternative splicing disrupts gene expression in auditory hair cells, leading to deafness, and targeting *REST*'s partners with HDAC inhibitors can rescue hearing in *Rest* mutant mice.

Highlights

- Alternative splicing of *REST* exon 4 regulates gene expression in hair cells
- A *REST* mutation is associated with defective exon 4 splicing and deafness in humans
- Genetic deletion of exon 4 of mouse *Rest* causes sensory hair cell loss and deafness
- The HDAC inhibitor SAHA (Vorinostat) rescues hearing in *Rest* mutant mice

Defects in the Alternative Splicing-Dependent Regulation of REST Cause Deafness

Yoko Nakano,^{1,2} Michael C. Kelly,^{3,9} Atteeq U. Rehman,^{4,5,9} Erich T. Boger,⁶ Robert J. Morell,⁶ Matthew W. Kelley,³ Thomas B. Friedman,⁴ and Botond Bánfi^{1,2,7,8,10,*}

¹Department of Anatomy and Cell Biology, Carver College of Medicine, University of Iowa, Iowa City, IA 52242, USA

²Inflammation Program, Carver College of Medicine, University of Iowa, Iowa City, IA 52242, USA

³Laboratory of Cochlear Development, National Institute on Deafness and Other Communication Disorders, NIH, Bethesda, MD 20892, USA

⁴Laboratory of Molecular Genetics, National Institute on Deafness and Other Communication Disorders, NIH, Bethesda, MD 20892, USA

⁵Department of Molecular and Human Genetics, Baylor College of Medicine, Houston, TX 77030, USA

⁶Genomics and Computational Biology Core, National Institute on Deafness and Other Communication Disorders, NIH, Bethesda, MD 20892, USA

⁷Department of Otolaryngology—Head and Neck Surgery, Carver College of Medicine, University of Iowa, Iowa City, IA 52242, USA

⁸Department of Internal Medicine, Carver College of Medicine, University of Iowa, Iowa City, IA 52242, USA

⁹These authors contributed equally

¹⁰Lead Contact

*Correspondence: botond-banfi@uiowa.edu

<https://doi.org/10.1016/j.cell.2018.06.004>

SUMMARY

The DNA-binding protein REST forms complexes with histone deacetylases (HDACs) to repress neuronal genes in non-neuronal cells. In differentiating neurons, REST is downregulated predominantly by transcriptional silencing. Here we report that post-transcriptional inactivation of REST by alternative splicing is required for hearing in humans and mice. We show that, in the mechanosensory hair cells of the mouse ear, regulated alternative splicing of a frameshift-causing exon into the *Rest* mRNA is essential for the derepression of many neuronal genes. Heterozygous deletion of this alternative exon of mouse *Rest* causes hair cell degeneration and deafness, and the HDAC inhibitor SAHA (Vorinostat) rescues the hearing of these mice. In humans, inhibition of the frameshifting splicing event by a novel REST variant is associated with dominantly inherited deafness. Our data reveal the necessity for alternative splicing-dependent regulation of REST in hair cells, and they identify a potential treatment for a group of hereditary deafness cases.

INTRODUCTION

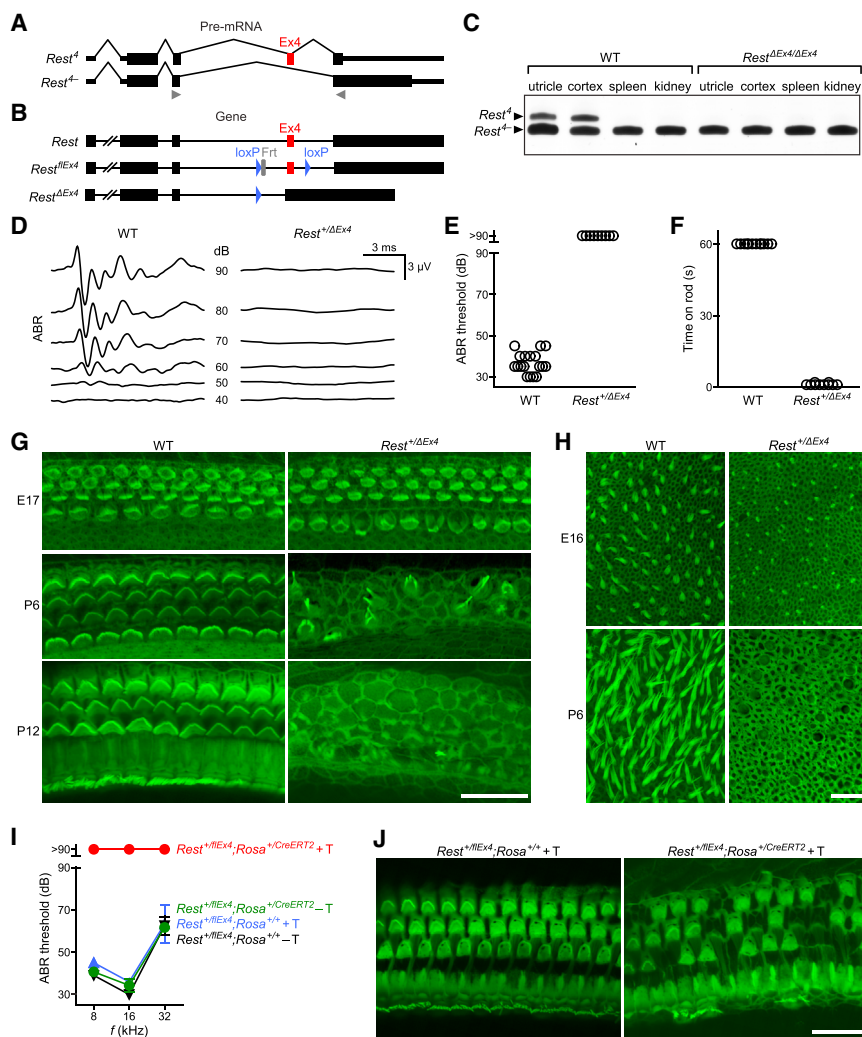
Repressor Element-1 (RE1) motifs are 21- to 30-bp DNA sequences located predominantly in neuronal genes, and they serve as binding sites for the RE1-silencing transcription factor (REST), also known as neuron-restrictive silencing factor (NRSF) (Chong et al., 1995; Schoenherr and Anderson, 1995). In non-neuronal cells, REST and its corepressors, coREST, histone deacetylase (HDAC)1, HDAC2, lysine-specific demethylase (LSD)1, and G9a methyltransferase (McGann et al., 2014), are vital to the repression of RE1-containing genes. In mice, ubiqui-

tous deletion of both *Rest* alleles (*Rest*^{-/-}) causes upregulation of neuronal transcripts in non-neuronal tissues and embryonic lethality (Chen et al., 1998), and conditional deletion of both *Rest* alleles in the common progenitors of glia and neurons causes genomic instability and premature expression of neuronal transcripts (Nechiporuk et al., 2016). Thus, REST plays two key roles in non-neuronal cells: repressing neuronal genes and protecting genomic stability.

REST protein expression is reduced dramatically in differentiating neurons. Given that no gain-of-function mutation in *REST* has been identified in any species, *in vivo* assessments of the importance of such reductions have been based on the delivery of constitutively transcribed *REST* constructs into the CNS of mouse and chick embryos. In these studies, electroporation of CNS neurons with *REST*-encoding expression plasmids led to errors in commissural axon guidance in the spinal cord and stalled radial migration in the neocortex (Paquette et al., 2000; Mandel et al., 2011).

Transcriptional repression is the main mechanism whereby REST is downregulated in differentiating neurons (Ballas et al., 2005); however, REST is also inactivated through alternative splicing of its pre-mRNA in both neurons and mechanosensory hair cells of the ear (Raj et al., 2011; Nakano et al., 2012). The contribution of this splicing event to the reduction of REST activity was not determined in any tissue prior to this study, and its impact on organ function has not been evaluated.

Alternative splicing produces forms of the *REST* mRNA that either contain or lack exon 4. Incorporation of this exon into the *REST* mRNA requires SRRM4, a splicing regulator expressed selectively in neurons and hair cells (Calarco et al., 2009; Nakano et al., 2012). Notably, the position of the splice acceptor site of exon 4 is not identical in all mammals, and thus the length of this exon is not uniform across species. In mice, exon 4 is a 16-nt frameshift-causing exon (Raj et al., 2011) (Figure 1A), whereas in humans two alternative splice donor sites exist and two forms of the exon are produced (Palm et al., 1999). Splicing of human *REST* at a donor site that is conserved between mice



Pure-tone stimuli were applied at the frequencies indicated (n = 5 mice/group). Values are mean ± SEM. (J) F-actin-stained organ of Corti preparations from control (*Rest*^{+/flEx4}, *Rosa*^{+/+}) and *Rest*^{+/flEx4}, *Rosa*^{+/-CreERT2} mice at P79, following treatment with tamoxifen from P40 to P47. Scale bar, 20 μm.

See also Figures S1, S2, and S3.

and humans produces a 50-nt exon with a stop codon (exon 4a), and splicing of human *REST* at a non-conserved donor site produces a 4-nt frameshifting microexon (exon 4b). Although all exon 4-containing *REST* transcripts encode inactive proteins that lack a repressor and three zinc-finger domains of the full-length isoform (Magin et al., 2002), exon 4 is rarely considered in analyses of the *REST* exon-intron structure, perhaps because none of the vertebrate genomes in the RefSeq database are annotated for it.

Here we set out to determine whether inactivation by alternative splicing is redundant with other mechanisms of *REST* regulation. We found that mice heterozygous for exon 4 deletion have no apparent CNS defects but lose all mechanosensory hair cells in the ear and fail to respond to sound. The exceptional sensitivity of the ear to exon 4 deletion correlated with the particularly high contribution of exon 4 splicing to *REST* downregulation in hair cells. Hair cells and hearing of exon 4-knockout mice were

rescued by treatment with SAHA (Vorinostat), an FDA-approved inhibitor of HDACs. Finally, analysis of the cause of dominantly inherited deafness in humans whose hearing loss was linked to the *REST*-containing *DFNA27* locus (Peters et al., 2008) revealed a novel variant of *REST* that prevented exon 4b-dependent inactivation of the encoded protein. Our data indicate that alternative splicing is essential for *REST* regulation in the inner ear and that defects in this mechanism can be offset by HDAC inhibitors.

RESULTS

Rest Exon 4 Is Necessary for the Development and Maintenance of Mechanosensory Hair Cells

We used homologous recombination in embryonic stem cells (ESCs) to generate mice heterozygous for a *Rest* allele in which exon 4 is flanked by loxP sites (*Rest*^{+/flEx4}; Figures 1B, S1A, and S1B). RT-PCR analysis of the neocortex of homozygous

Figure 1. Rest Exon 4 Is Critical for Hearing in Mice

(A) Schematic of exon-intron structures of *Rest* isoforms, illustrating differences in lengths of reading frames between the exon 4-containing (*Rest*^{+/+}) and exon 4-omitting (*Rest*^{−/+}) splice forms. Constitutively spliced exons (black rectangles), exon 4 (Ex4, red), and UTRs (thin rectangles) are indicated. Tented lines represent joining of exons in maturing pre-mRNA. Gray arrowheads show positions of RT-PCR primers used in experiments depicted in (C).

(B) Schematic of wild-type (*WT*) *Rest*, an exon 4-flanked form of *Rest* (*Rest*^{flEx4}), and an exon 4-deleted form of *Rest* (*Rest*^{ΔEx4}). Exons and introns are indicated as in (A). Blue and gray symbols represent loxP and Frt sites, respectively.

(C) RT-PCR analysis of exon 4 splicing in the indicated tissues of *WT* mice and mutant mice homozygous for the dominant *Rest*^{ΔEx4} allele. RNA was isolated at E15.5 (utricle) and P0 (other tissues). Spleen and kidney are shown as examples of non-neuronal tissues.

(D) Representative ABR waveforms for *WT* and *Rest*^{+/ΔEx4} mice at P28. Broadband click stimuli were applied at sound pressure levels indicated in decibels.

(E) Thresholds of broadband click-evoked ABRs of *WT* and *Rest*^{+/ΔEx4} mice at P28. Each symbol represents value for a single mouse.

(F) Time spent on a horizontal rod before falling for *WT* and *Rest*^{+/ΔEx4} mice at P21–P28. Maximal duration of the assay was 60 s.

(G and H) Organ of Corti (G) and utricle (H) preparations from *WT* and *Rest*^{+/ΔEx4} mice at the indicated developmental stages, stained with phalloidin-Alexa488 to visualize F-actin-rich structures, including stereocilia and cell-cell borders. Scale bars, 20 μm.

(I) ABR thresholds of P70–P80 control (*Rest*^{+/flEx4}, *Rosa*^{+/+T}) and *Rest*^{+/flEx4}, *Rosa*^{+/-T} mice treated with tamoxifen (+T) or solvent (-T) from P40 to P47.

Rest^{flox4/flox4} and wild-type (WT) mice demonstrated that insertion of loxP sites did not affect splicing of exon 4 into the mRNA (Figures S1C and S1D). An exon 4-deleted form of *Rest* (*Rest*^{-ΔEx4}) was created by crossing *Rest*^{flox4/flox4} mice to transgenic mice expressing Cre recombinase under the control of a ubiquitously active β -actin promoter (Figures 1B and S1E). RT-PCR analysis of neural and non-neuronal tissues of *Rest*^{-ΔEx4} and WT mice confirmed that this deletion prevented production of the exon 4-containing splice form (*Rest*⁴) without reducing expression of the form lacking this exon (*Rest*⁻⁴; Figures 1C and S1F).

Heterozygous *Rest*^{+/-ΔEx4} mice exhibited balance defects and were deaf (Figures 1D–1F). Histological analysis of the inner ear of *Rest*^{+/-ΔEx4} mice revealed that hair cells were present until embryonic day (E)16–E17 but degenerated throughout the inner ear by post-natal day (P)12 (Figures 1G, 1H, S1G, S1H, and S2). The autonomy of the hair cell defect was tested by intercrossing the *Rest*^{+/-ΔEx4} mice to *Gfi1*^{+/Cre} mice, which express Cre selectively in hair cells (Yang et al., 2010). As in the case of global heterozygous deletion of exon 4, hair cell-specific deletion of one copy of exon 4 led to the degeneration of hair cells (Figure S1I) and deafness (data not shown). Thus, *Rest* exon 4 is essential for hair cell development and this function is cell autonomous.

Next, we tested whether deleting one copy of *Rest* exon 4 when the ear is fully developed affects hearing. *Rest*^{flox4/flox4} mice were crossed to mice homozygous for a transgene encoding tamoxifen-inducible Cre recombinase in the Rosa26 locus (*Rosa*^{CreERT2/CreERT2}), and the offspring were treated with tamoxifen or control vehicle from P40 to P47. One month later, measurement of auditory brainstem responses (ABRs) to various pure-tone stimuli revealed hearing loss in the tamoxifen-injected *Rest*^{+/-ΔEx4}; *Rosa*^{+/CreERT2} mice, but not in vehicle-injected mice of the same genotype (Figure 1I). Histological analyses of the inner ear of tamoxifen-injected *Rest*^{+/-ΔEx4}; *Rosa*^{+/CreERT2} mice revealed partial loss of hair cells (Figures 1J and S3A), and PCR testing of the organ of Corti demonstrated that tamoxifen-dependent recombination occurred in some copies of the *Rest*^{flox4} allele (Figure S3B), consistent with reports of mosaic Cre activation in other organs (Hameyer et al., 2007). Thus, *Rest* exon 4 is critical for hair cell survival in both newborn and adult mice.

Immunofluorescence analysis of the hearing organ of P6 *Rest*^{+/-ΔEx4} mice revealed expression of the active form of the pro-apoptotic executioner caspase-3 in many hair cells (Figure S3C). Activation of the apoptotic pathway was confirmed by the fact that the caspase inhibitors Z-DEVD-FMK and Z-VAD-FMK delayed the death of hair cells in organ of Corti cultures derived from *Rest*^{+/-ΔEx4} mice. However, these inhibitors failed to prevent the degeneration of stereocilia (Figures S3D and S3E), suggesting that the inhibition of apoptosis is insufficient to rescue hair cells of *Rest*^{+/-ΔEx4} mice.

Although *Rest* is alternatively spliced in the developing neocortex, H&E staining of brain sections from *Rest*^{+/-ΔEx4} mice did not reveal pathological alterations (Figure S3F). The lack of histological defects in the CNS was further supported by immunostaining of brain sections from newborn *Rest*^{+/-ΔEx4} mice with antibodies against markers of various cortical layers (Figures S3G–S3I), as well as by immunostaining of neural tubes of

such mice with an antibody against the commissural axon marker TAG-1 (Figure S3J). Thus, *Rest* exon 4 is not essential for either radial migration in the neocortex or commissural axon pathfinding in the spinal cord.

An Intrinsic C > G Variant in Human REST Is Associated with Progressive Hearing Loss

We previously mapped dominantly inherited postlingual progressive hearing loss in a family (LMG2) to the *REST*-containing DFNA27 segment of chromosome 4 (Peters et al., 2008). The DFNA27 locus encompasses seven annotated genes in addition to *REST*. Sequencing of all annotated exons in the DFNA27 locus of affected individuals failed to identify potentially pathogenic variants (data not shown), but sequencing of conserved intronic regions of *REST* revealed a C > G variant 21 bases upstream of exon 4a/b (chromosome [chr]4:56,927,594 in GRCh38 assembly; Figure 2A). This intronic variant co-segregated with hearing loss in the LMG2 family (Figure 2B). The outcomes of three additional analyses were consistent with the notion that the C > G variant is pathogenic: the C nucleotide is conserved in all 80 genomes listed in the UCSC Genome Browser as containing a region similar to exon 4 of *REST*, the G variant is absent from the Genome Aggregation Database, and sequencing of 400 DNA samples (Coriell Human Diversity Panel) invariably detected C 21 bases upstream of exon 4a/b. Thus, a rare sequence variant in the third intron of *REST* co-segregates with hearing loss in the LMG2 family.

The C > G variant causes an AC-to-AG change downstream of a polypyrimidine tract, a sequence combination that is the hallmark of splice acceptor sites. To determine whether the AG sequence affects *REST* splicing, we performed RT-PCR analysis of blood cell RNA for a control and 2 affected subjects. RT-PCR amplification of the exon 3–5 junction region of the *REST* mRNA produced a single product for the control subject but two for the affected subjects (Figure 3A). The longer product, which was observed only for the affected subjects, contained a mutant form of exon 4a (designated exon 4a^M) with an in-frame stop codon. The splice acceptor site of exon 4a^M was at the variant AG sequence, and the splice donor site was identical to that of exon 4a (Figure 3E). The shorter product was identified as the amplicon of the WT *REST*⁻⁴ mRNA (Figures 3A and 3B). Thus, the C > G variant causes truncation of the coding region of *REST* in a non-neuronal tissue by generating a novel splice acceptor site for exon 4a. However, heterozygosity for the exon 4a^M-dependent inactivation of *REST* is unlikely to explain the DFNA27 phenotype, because the hearing threshold of heterozygous *Rest* knockout (*Rest*^{+/-}) mice (Gao et al., 2011) is similar to that of WT littermates at P130 (Figure S3K). Thus, we tested the C > G DFNA27 variant for additional defects in *REST* pre-mRNA processing in the presence of SRRM4, which regulates alternative splicing of exon 4.

The Intrinsic C > G Variant Prevents SRRM4-Dependent Inactivation of REST

Splicing of exon 4 into the *REST* mRNA is normally tissue specific and requires SRRM4, which is expressed selectively in neurons and hair cells. SRRM4 binds to pre-mRNAs at

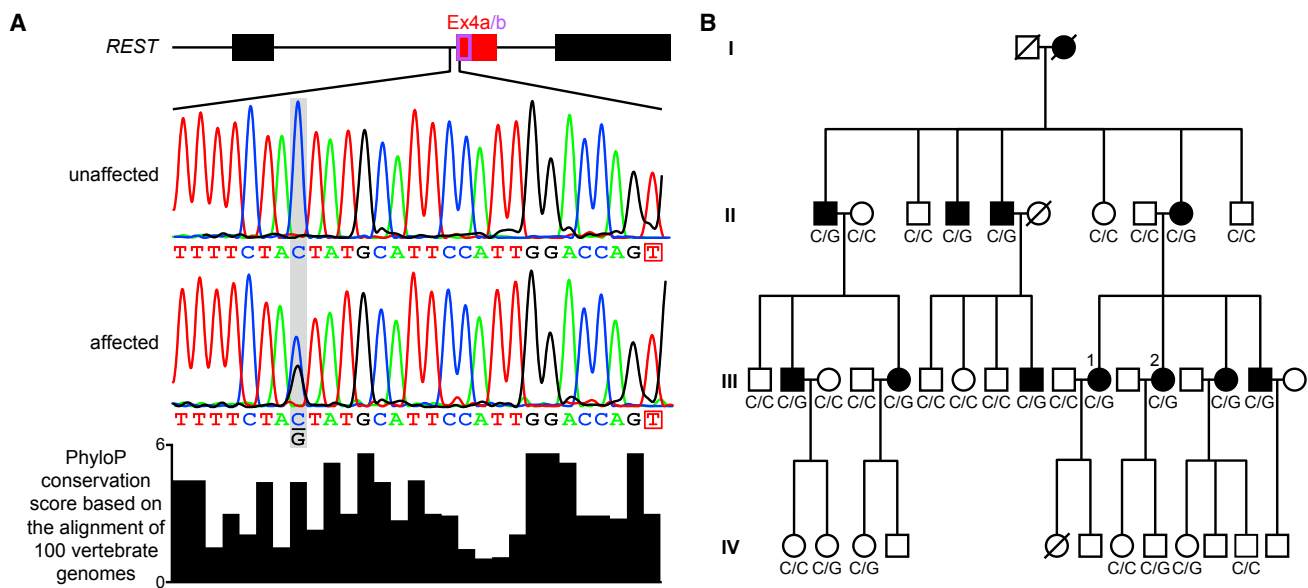


Figure 2. DFNA27 Contains an Intronic C > G Variant near REST Exon 4

(A) Location and conservation of *REST* region containing a C > G variant in family LMG2. Top: schematic of exon-intron structure of *REST* from exon 3 to exon 5 is shown. Rectangles indicate exons 3 and 5 (black), exon 4a (red), and exon 4b (purple outline). Introns are shown as horizontal lines. Middle: chromatograms depict genomic sequences upstream of exon 4a/b in an unaffected and an affected heterozygous subject. In the affected subject, the wild-type C nucleotide in intron 3 of *REST* is replaced by a G (gray shading). First base of exon 4a/b is boxed. Bottom: vertebrate PhyloP conservation score is shown.

(B) Pedigree of LMG2 family, showing co-segregation of progressive hearing loss with intronic C > G variant of *REST*. Filled symbols represent individuals with hearing loss; hearing data are not available for generation IV. Letters beneath symbols indicate nucleotides 21 bases upstream of *REST* exon 4 in the individual. Arabic numerals identify subjects whose RNA was analyzed (Figure 3A).

UGC motifs located between polypyrimidine tracts and downstream alternative exons (Nakano et al., 2012; Raj et al., 2014), and when it does so the alternative exon is incorporated into the mature mRNA. We used minigenes to test the effects of SRRM4 on alternative splicing of the C > G DFNA27 variant of *REST*. WT and DFNA27 versions of the minigene were created by inserting *REST* exon 4a/b and its flanking introns, from a control subject and an affected subject, respectively, between two constitutively spliced exons (Figure 3C, top). The non-neuronal cell line HEK293 was co-transfected with the minigene and either an SRRM4-encoding plasmid or an empty control expression vector. Splicing of the minigene-encoded transcript in transfected cells was analyzed by RT-PCR using primers that annealed to the constitutive exons of the minigenes. In the absence of SRRM4 expression, RNA encoded by the WT minigene contained only constitutive exons (splice form 4-) and RNA encoded by the DFNA27 minigene contained exon 4a^M. In the presence of SRRM4, two splice forms were expressed from the WT minigene: one containing exon 4a and another containing the exon 4b microexon (Figures 3C–3E). The ratio of exon 4a- and exon 4b-containing splice forms was approximately 6 to 1 in the transfected cells; a similar ratio of exon 4a- and exon 4b-containing *REST* transcripts was detected in human fetal brain (Figures S3L and S3M). In the presence of SRRM4, two RNA splice forms were also expressed from the DFNA27 minigene: an exon 4a^M-containing form (longer), and a novel form that contained a 24-nt variant of

exon 4b (i.e., exon 4b^M; shorter). The splice acceptor site of exon 4b^M was at the DFNA27-specific AG, and its splice donor site was identical to that of exon 4b (Figures 3D–3F). Thus, the splicing of exon 4b^M required both C > G variant-dependent relocation of the splice acceptor site and an SRRM4-dependent shift in the splice donor site. Exon 4b^M encodes 8 amino acids and does not alter the reading frame (Figure 3E). We hypothesized that inclusion of exon 4b^M in the *REST* mRNA leads to the production of a functional REST^{4bM} protein.

To test the gene repressor activity of each REST isoform, we co-transfected Neuro2a cells (which contain little endogenous REST) with it and a reporter of REST activity. The reporter contains an RE1 sequence upstream of a luciferase expression cassette (Figure 3G). Immunoblot analysis of the transfected cells demonstrated comparable expression of the REST isoforms (Figure S3N). Measurement of luciferase activity (Figure 3G) revealed that 2 of 5 isoforms were active: the REST⁴⁻ form, which was produced only in the absence of SRRM4; and the aberrant REST^{4bM} form, which was produced only in SRRM4-expressing cells and in the presence of the C > G DFNA27 variant. These data suggest that the C > G DFNA27 variant has opposing effects on REST depending on whether or not SRRM4 is present. In cells that do not express SRRM4, the C > G variant inactivates REST aberrantly by creating a novel acceptor site for constitutive splicing upstream of exon 4a/b. In cells that do express SRRM4, the C > G variant aberrantly leads to the production of active REST, because no stop codon

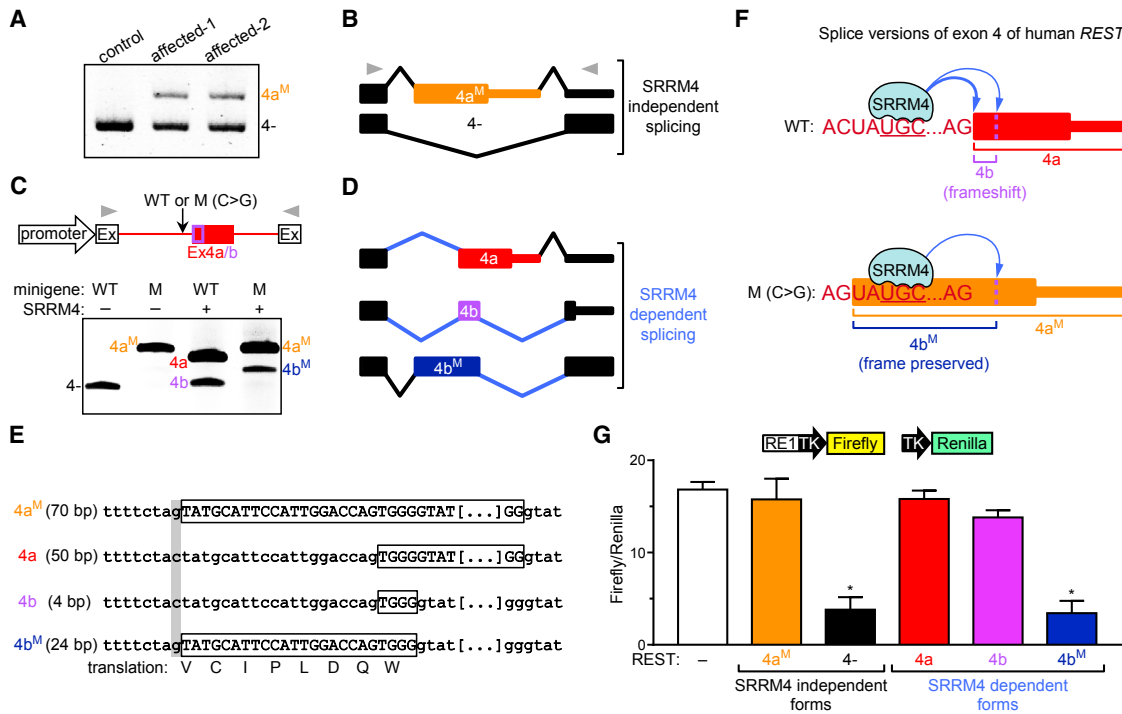


Figure 3. C > G DFNA27 Variant Prevents Alternative Splicing-Dependent REST Inactivation

(A) RT-PCR for the detection of *REST* splice forms in blood cells from two affected subjects (indicated by numbers in Figure 2B) and a control subject. Locations of PCR primers are shown in (B) (gray arrowheads). 4a^M and 4- indicate detected mutant and wild-type (WT) splice forms, respectively.

(B) Schematic of splice site selection in 4a^M and 4- splice forms shown in (A). SRRM4-independent splicing refers to a lack of SRRM4 in blood cells. Constitutively spliced exons 3 and 5 (black rectangles), exon 4a^M (orange), and UTRs (thin rectangles) are indicated. Tented lines represent joining of exons in pre-mRNA.

(C) RT-PCR testing of effect of C > G variant on splicing of exons 4a/b in HEK293 cells co-transfected with a *REST* minigene and an SRRM4-encoding plasmid or empty vector. Top: schematic of minigenes is shown, with constitutively spliced exons (Ex) flanking WT or DFNA27 (mutant [M]) version of exon 4a/b (Ex4a/b)-containing *REST* segment. Minigene promoter, positions of RT-PCR primers (arrowheads), and mutation site (vertical arrow) are indicated. Bottom: 4-, 4a, and 4b represent detected WT splice forms; 4a^M and 4b^M represent detected mutant splice forms.

(D) Schematic of SRRM4-dependent splice site selection (blue lines) in 4a, 4b, and 4b^M splice forms shown in (C).

(E) Sequences (boxed) and lengths (bp) of indicated exon 4 splice forms. Gray shading indicates site of mutation. Translation line shows amino acids encoded by exon 4b^M.

(F) Illustrations of effects of SRRM4 on splice sites (curved arrows) and reading frames in transcripts encoded by WT and DFNA27 (mutant [M]) *REST* forms. Vertical dotted lines indicate SRRM4-dependent splice donor site. UGC core of SRRM4-binding motif is underlined.

(G) Expression levels of REST-binding site (RE1)-containing reporter gene in Neuro2a cells transfected with empty vector (–) or indicated *REST* splice form. Schematic at top shows compositions of Firefly reporter and Renilla control constructs. Values are mean ± SEM; n = 4 independent assays; one-way ANOVA, p < 0.0001; post hoc Dunnett's test, *p < 0.0001 (control group, –). TK, thymidine kinase gene promoter.

See also Figure S3.

is present in the 24-base region between the C > G variant-generated splice acceptor site and SRRM4-dependent splice donor site of exon 4b^M. Our results strongly suggest that SRRM4-directed alternative splicing of exon 4 cannot inactivate REST in human subjects whose genome harbors the C > G DFNA27 variant.

The *Rest*^{ΔEx4} Mutation Is Associated with Abnormally High REST Activity in the Ear

We used the *Rest*^{+/ΔEx4} mouse to identify exon 4-dependent alterations in the inner ear transcriptome at E15.5, a time corresponding to the onset of hair cell degeneration in the mutant mice (Figure S2C). RNA was isolated from the utricle, because in *Rest*^{+/ΔEx4} mice the onset of hair cell degeneration in this structure is more synchronous than in the cochlea. RNA sequencing

(RNA-seq) analysis of utricular samples identified 357 genes that are differentially expressed in *Rest*^{+/ΔEx4} and WT mice (Figure 4A; Table S1). Analysis of the same data for alternative splicing patterns of mRNAs other than *Rest* did not reveal differences between the two groups (Figure S4A). Thus, the *Rest*^{+/ΔEx4} genotype is associated with changes in utricular gene expression.

To identify REST targets among the differentially expressed genes, we used a filtered set of REST chromatin immunoprecipitation sequencing (ChIP-seq) data from the Encyclopedia of DNA Elements (ENCODE) (STAR Methods), and we located REST-binding sites in 744 genes across the genome (Table S2). We refer to the 744 genes as high-confidence REST targets. Among 357 genes differentially expressed in the utricles of WT and *Rest*^{+/ΔEx4} mice, 64 were high-confidence REST targets

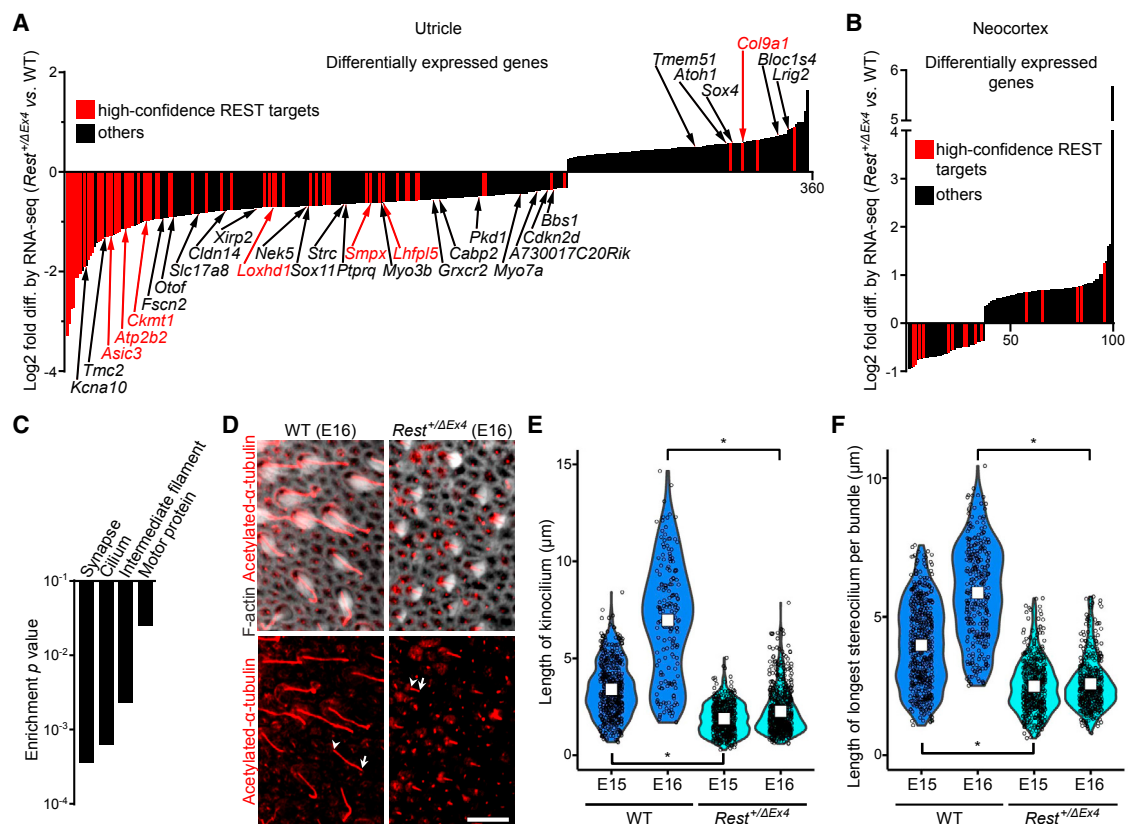


Figure 4. Genomic Deletion of Exon 4 of Mouse Rest Is Associated with Reduced Expression of Many Hearing-Related Genes

(A) Differences in gene expression between utricles of WT and Rest^{+/ΔEx4} mice at E15.5. Red bars indicate high-confidence REST target genes. Arrows and names indicate differences in expression levels of genes known to be important for hearing or balance. Names of all differentially expressed genes are listed in Table S1. (B) Differences in gene expression between the neocortices of WT and Rest^{+/ΔEx4} mice at E15.5. Color coding is the same as in (A); gene names are listed in Table S4.

(C) Enrichment of Uniprot keyword annotations in set of genes differentially expressed in the Rest^{+/ΔEx4} versus WT mouse utricle.

(D) Representative images of stereocilia (F-actin staining, white bundles) and kinocilia (acetylated α-tubulin immunostaining, red strips) in the utricles of Rest^{+/ΔEx4} and WT mice at E16. For two kinocilia, tip (arrow) and base (arrowhead) are indicated in lower panels. Scale bar, 10 μm.

(E and F) Violin plots of lengths of kinocilia (E) and maximum lengths of stereocilia bundles (F) in WT and Rest^{+/ΔEx4} mouse utricular hair cells at E15 and E16. Each circle represents one kinocilium (E) or longest stereocilium (F) of a hair cell (pooled data from 6 utricles of 3 mice/group). White rectangles indicate means. Mann-Whitney test, false discovery rate (FDR) adjusted, *p < 0.0001.

See also Figure S4 and Tables S1, S2, S3, and S4.

(red bars in Figure 4A; Table S1). The set of high-confidence REST target genes represented 25% of all genes that are expressed at reduced levels in the utricles of Rest^{+/ΔEx4} mice; such genes represent only 3.6% of all genes expressed in hair cells (Scheffer et al., 2015) (Fisher's exact test, p < 0.0001; further analyses in Figures S4B and S4C). Thus, the expression of several high-confidence REST targets is abnormally low in the utricles of Rest^{+/ΔEx4} mice at the onset of hair cell degeneration.

Searches of various genotype-phenotype databases (Table S1) revealed that disorders of hearing or balance have been linked to 31 of the genes that we found to be differentially expressed in the utricles of Rest^{+/ΔEx4} and WT mice (Figure 4A). Furthermore, 20 of these are required specifically for hair cell development and function (Table S1). Thus, incorporation of exon 4 into Rest is necessary for the regulation of several genes that encode proteins critical for the development and function of hair cells.

Heterozygous Deletion of Rest Exon 4 Causes Defects in the Cilia of Utricles

Our analysis of Uniprot keyword annotations of genes expressed at reduced levels in the utricles of Rest^{+/ΔEx4} mice revealed the lowest p values to be associated with the keywords synapse and cilium (Figure 4C). Although REST was known to regulate the expression of many synaptic proteins (Ballas et al., 2005), it had not been linked to ciliogenesis. A review of genes associated with the keyword cilium showed that 12 stereocilium-related and 37 kinocilium-related genes are expressed at reduced levels in the utricles of Rest^{+/ΔEx4} mice (Table S1). High-confidence REST targets were more frequent among the stereocilium-related (25%) versus kinocilium-related (8%) genes.

Given that RFX2–4 and RFX7 regulate the transcription of many kinocilium-related genes (Manojlovic et al., 2014), we examined the differentially expressed genes and all hair cell-expressed genes for evolutionarily conserved sequences similar

to RFX-binding motifs. Such sequences were present in 23% of genes expressed at reduced levels in the utricles of *Rest*^{+/ΔEx4} mice but in only 9.6% of all genes expressed in utricular hair cells (Fisher's exact test, $p < 0.0001$; **Tables S1** and **S3**; **Figures S4D** and **S4E**). These data suggest that alternative splicing of *Rest* affects utricular expression of several RFX targets. Our RNA-seq and qRT-PCR analyses also revealed reduced expression of *Rfx7* in the utricle of *Rest*^{+/ΔEx4} mice (**Figure S4C**). Although *Rfx7* is not a high-confidence REST target, an RE1-like sequence from this gene conferred REST-dependent repression to a reporter (**Figures S4F** and **S4G**). These data are consistent with REST modulating the expression of an RFX family transcription factor in the ear.

We next examined cilia in the utricles of *Rest*^{+/ΔEx4} and WT mice at E15 and E16. Stereocilia were identified by F-actin staining, and kinocilia were labeled using an antibody against acetylated α -tubulin. Confocal microscopy revealed that both organelles were abnormally short in the utricles of *Rest*^{+/ΔEx4} mice at E15 and E16 (**Figures 4D–4F**). Thus, the abnormally low expression of many stereocilium- and kinocilium-related genes in the utricles of *Rest*^{+/ΔEx4} mice is associated with the shortening of both organelles.

Contributions of Alternative Splicing and Transcriptional Repression to REST Downregulation Differ between Hair Cells and Cortical Neurons

We assessed the effect of the *Rest*^{ΔEx4} mutation on gene expression in the neocortex, which we selected as a reference neural tissue. RNA-seq analysis of neocortices of E15.5 WT and *Rest*^{+/ΔEx4} mice revealed differential expression of 100 genes (**Figure 4B**). Among these, 15 were high-confidence REST targets, and expression of 10 of the 15 was moderately (i.e., <2-fold; **Table S4**) reduced in the *Rest*^{+/ΔEx4} neocortex. For high-confidence REST targets randomly selected from the cortical and utricular RNA-seq datasets, qRT-PCR analysis at additional time points demonstrated that expression in the *Rest*^{+/ΔEx4} neocortex was reduced at E16, but not P6 and P16 (**Figure S4H**). In contrast, expression in the utricle and saccule was reduced even at P16 following tamoxifen-induced deletion of exon 4 at P7–P9 (**Figures S4H** and **S4I**). These data suggest that the impact of exon 4 splicing on the expression of high-confidence REST targets differs between hair cells and cortical neurons, with respect to both magnitude and duration.

RT-PCR analysis of *Rest* exon 4 splicing showed that, whereas the *Rest*⁴⁺:*Rest*⁴⁻ ratio declined between E16 and P16 in the neocortex, it did not decline after birth in the inner ear (**Figure 5A**). Given that exon 4 is not spliced into *Rest* in non-neuronal cells, the *Rest*⁴⁺:*Rest*⁴⁻ ratio is likely affected by the relative numbers of neuronal versus non-neuronal cells in the analyzed tissue. Thus, we chose to evaluate *Rest* promoter activity on a cell-by-cell basis. We used a mouse line that harbors a *Rest* promoter-EGFP transgene ([Gong et al., 2003](#)), in which an EGFP-coding sequence is present downstream of the *Rest* start codon (**Figure 5B**). The activity of the transgenic *Rest* promoter was evaluated based on the intensity of EGFP immunofluorescence in sections of the neocortex and inner ear. Neurons and hair cells were identified using anti-NeuN and anti-MYO7A antibodies, respectively. In cortical sections from P0 transgenic

mice, the EGFP signal varied among individual neurons, representing from 2% to 60% of the EGFP signal in non-neurons. By P16, the neuronal EGFP signal was reduced to 0.4%–7% of that in non-neurons (**Figures 5C** and **5E**). In the ear, the EGFP signal in inner hair cells (IHCs) and utricular hair cells at both P0 and P16 was still 50% that in non-hair cells (non-HCs; **Figures 5D** and **S4J**); in outer hair cells (OHCs) the signal increased between P0 and P16 (**Figure 5E**). These data suggest that promoter-dependent downregulation of *Rest* is much stronger in cortical neurons than hair cells.

Single-Cell qRT-PCR Identifies Alternative Splicing as a Major Mechanism of REST Inactivation in Hair Cells

Given that hair cells were not previously evaluated for *Rest* expression, we used a second approach to confirm the transgene-based assessment of *Rest* transcription in the hearing organ. Multiplex single-cell qRT-PCR (scqRT-PCR) was selected because it has the potential to reveal changes in both the expression and splicing of *Rest* in individual cells. Single cells from enzymatically dissociated organs of Corti of P1 and P7 WT mice were captured on fluidics circuits and lysed. Following reverse transcription, a specific set of cDNA targets was quantified by multiplex qPCR. The set of quantified cDNA segments included a region shared by *Rest*⁴⁺ and *Rest*⁴⁻ (i.e., total *Rest*), the exon 4–5 junction region unique to *Rest*⁴⁺, and the exon junction regions of several cell-type-specific transcripts (for assignment of cell type). This analysis revealed that at P7 total *Rest* expression was comparable in non-HCs, IHCs, and OHCs, whereas at P1 it was comparable in only non-HCs, IHCs, and a subset (70%) of OHCs (**Figure 5F**). In the remaining 30% of P1 OHCs the *Rest* mRNA was undetectable. This analysis also revealed that 94% of *Rest*-expressing hair cells, but fewer than 1% of non-HCs, contained the *Rest*⁴⁺ splice form (**Figure 5F**). Thus, *Rest* expression was high in IHCs and upregulated in OHCs during the first post-natal week. In addition, the *Rest*⁴⁺ splice form was specific to hair cells in the organ of Corti.

The single-cell cDNAs were analyzed further by PCR to determine what percentage of *Rest* mRNAs in cochlear cells contain exon 4. At P1, ~70% of *Rest* mRNA in IHCs were *Rest*⁴⁺, whereas in OHCs both the expression and splicing of *Rest* were variable (**Figures 5F–5H**). By P7 all OHCs expressed *Rest* and 92%–100% of *Rest* mRNA in both IHCs and OHCs was the *Rest*⁴⁺ form, but in non-HCs *Rest*⁴⁻ was the only detected splice form. Thus, although the *Rest* gene is transcribed in all IHCs and OHCs by the end of the first post-natal week, expression of the exon 5-encoded segment of REST, which is critical to its repressor activity, was minimal due to the incorporation of exon 4 into the transcript. Overall, our expression data reveal differences in the regulation of REST in hair cells versus cortical neurons: transcriptional silencing is the predominant form of REST downregulation in cortical neurons, and alternative splicing (inclusion of exon 4) is the main mechanism of REST inactivation in hair cells.

HDAC Inhibitors Rescue OHCs of Rest Exon 4-Deficient Mice in Organ Cultures

Considering that HDAC1 and HDAC2 are critical for REST-dependent gene repression ([McGann et al., 2014](#)), we examined

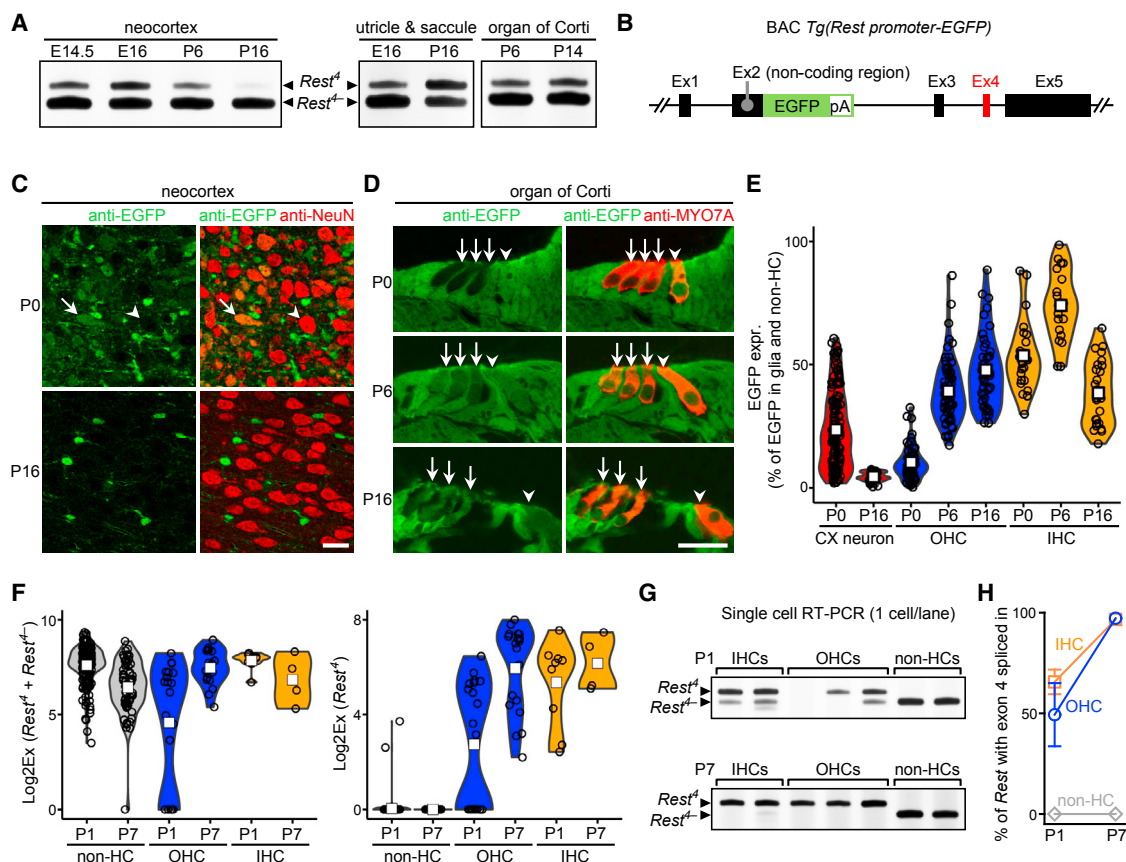


Figure 5. Contributions of Alternative Splicing and Transcriptional Silencing to the Downregulation of REST Activity Differ in Hair Cells and Cortical Neurons

- (A) RT-PCR analysis of Rest exon 4 splicing in the indicated tissues of WT mice.
 - (B) Schematic of BAC transgene engineered for quantification of Rest promoter activity. Transgene contains an EGFP reporter (green box) immediately downstream of Rest start codon. pA, polyadenylation signal. Exons and introns of Rest are indicated as in Figure 1B.
 - (C) EGFP (green) and NeuN (red) immunofluorescence in cortical sections from *Tg(Rest promoter-EGFP)* mice at P0 and P16. Examples of cells that are NeuN positive and either EGFP positive (arrow) or negative (arrowhead) are shown. Scale bar, 20 μm.
 - (D) EGFP (green) and MYO7A (red) immunofluorescence in cochlear sections from *Tg(Rest promoter-EGFP)* mice at P0, P6, and P16. Arrows, OHCs; arrowheads, IHCs. Scale bar, 20 μm.
 - (E) Violin plot of *Tg(Rest promoter-EGFP)* expression in cortical (CX) neurons, OHCs, and IHCs at the indicated times, as determined by immunofluorescence. EGFP signal was quantified as the percentage of that in non-neuronal cells and non-hair cells in the same sections. Each circle represents an individual cell. White rectangles indicate means.
 - (F) Violin plot of total Rest expression (left plot) and Rest⁺ expression (right plot) in the indicated cochlear cells at P1 and P7, as determined by scqRT-PCR. Each circle represents an individual cell. White rectangles indicate means.
 - (G) scRT-PCR analyses of splicing of Rest exon 4 in the indicated cochlear cells at P1 and P7.
 - (H) Quantification of Rest exon 4 splicing in single cells from organ of Corti in P1 and P7 mice. Splicing is quantified as the percentage of Rest transcripts containing exon 4 versus total Rest transcripts. Values are mean ± SEM; n = 4 IHCs from 3 mice at P1, 4 IHCs from 2 mice at P7, 8 OHCs from 3 mice at P1, and 10 cells from 3 mice/group in other groups.
- See also Figure S4.

the ability of HDAC inhibitors to modulate REST activity. We tested three inhibitors: FK228 (HDAC1–3, 10, and 11 selective) (Ganesan, 2015), SAHA (pan-HDAC), and Merck60 (HDAC1 and HDAC2 selective) (Methot et al., 2008). In HEK293 cell cultures, all three inhibitors increased the expression of nearly all eight REST targets that were selected for qRT-PCR analysis based on reduced expression of their orthologs in the ear and brain of the *Rest^{+/ΔEx4}* mouse (Figure S5A). Thus, the effects of FK228, SAHA, and Merck60 on the expression of REST target genes were similar to those of splicing exon 4 into Rest.

We used an organ culture system to test the effects of all three HDAC inhibitors on the hair cells of *Rest^{+/ΔEx4}* mice. Organ of Corti cultures from P1 *Rest^{+/ΔEx4}* and WT mice were incubated with 2 nM FK228, 1 μM SAHA, 1.2 μM Merck60, or solvent (non-treated group) from the second day *in vitro* (DIV2) to DIV8. F-actin staining of these cultures at DIV9 revealed that, whereas in non-treated organ cultures from *Rest^{+/ΔEx4}* mice the stereocilia of most OHCs degenerated, in HDAC inhibitor-treated cultures from the same mouse line most OHCs retained stereocilia (Figures 6A, 6B, and S5B).

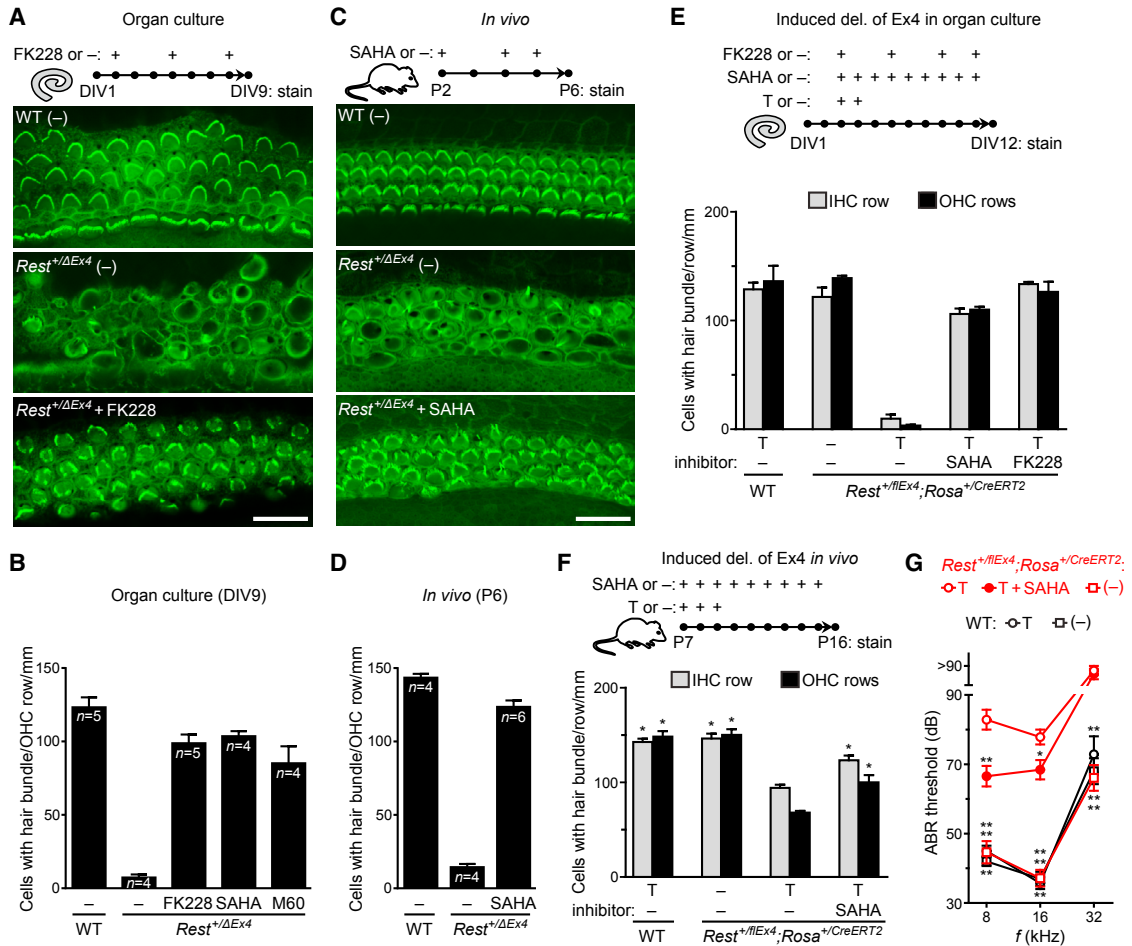


Figure 6. HDAC Inhibitors Rescue Hair Cells and Hearing of Rest Exon 4 Knockout Mice

- (A) Effect of FK228 on OHC morphology in organ cultures from *Rest^{+/ΔEx4}* mice. Top: schematic of treatment of organs of Corti from P1 *Rest^{+/ΔEx4}* and WT mice is shown, from day *in vitro* 2 (DIV2) to DIV8 followed by visualization of F-actin on DIV9. Scale bar, 20 μ m; solvent control, -.
- (B) Numbers of cells with stereocilia bundles in OHC-containing regions of DIV9 organ of Corti cultures of the indicated genotypes and inhibitor treatments. Cultures were derived from P1 mice. Lack of stereocilia bundles served as an indicator of OHC degeneration. M60, Merck60. Values are mean \pm SEM; n, number of mice (1 culture/mouse/group).
- (C) F-actin-stained preparations of organs of Corti from SAHA- or vehicle-treated *Rest^{+/ΔEx4}* and WT mice at P6. Mice received SAHA or vehicle (-), as illustrated by the scheme at top. Scale bar, 20 μ m.
- (D) Numbers of OHCs with stereocilia bundles in middle turn of cochleas from *Rest^{+/ΔEx4}* and WT mice at the end of treatment schedule depicted in (C). Values are mean \pm SEM (n, number of mice).
- (E) Numbers of hair cells with stereocilia bundles in DIV12 organ of Corti cultures derived from WT and *Rest^{+/flEx4; Rosa^{+/-CreERT2}}* mice at P5. Tamoxifen (T), SAHA, FK228, or solvent (-) was added at the indicated times. Values are mean \pm SEM (n = 3 cultures from 3 mice/group).
- (F) Numbers of hair cells with stereocilia bundles in the middle turn of the cochleas of WT and *Rest^{+/flEx4; Rosa^{+/-CreERT2}}* mice, at the end of the depicted treatment schedule. Values are mean \pm SEM; n = 3 mice/group; two-way ANOVA, p < 0.0001; post hoc Dunnett's test, *p \leq 0.003; control group, *Rest^{+/flEx4; Rosa^{+/-CreERT2}}* + T.
- (G) ABR thresholds of P16 WT and *Rest^{+/flEx4; Rosa^{+/-CreERT2}}* mice treated with tamoxifen (T), SAHA, or vehicle, as indicated in (F). Values are mean \pm SEM; n = 8 mice in T + SAHA group; 7 mice/group in other groups. Two-way ANOVA, p < 0.0001; post hoc Dunnett's test, *p = 0.043 and **p \leq 0.0002; control group, *Rest^{+/flEx4; Rosa^{+/-CreERT2}}* + T.

See also Figures S5 and S6 and Table S5.

Thus, HDAC inhibitors prevented the degeneration of OHCs of *Rest^{+/ΔEx4}* mice *in vitro*.

Next, we analyzed the effects of FK228 on the transcriptomes of organ of Corti cultures. FK228 was selected for this experiment for two reasons: it inhibits fewer HDACs than SAHA, and it is available from multiple commercial resources while Merck60

is not. RNA-seq analysis of FK228-treated and non-treated organ of Corti cultures from *Rest^{+/ΔEx4}* and WT mice revealed treatment-dependent alterations in the expression of ~8,000 genes, independent of the genotype of the mouse of origin (Table S5). Among these genes, and also among the genes that were differentially expressed in the utricles of *Rest^{+/ΔEx4}* and WT mice,

those that were high-confidence REST targets or contained potential binding sites for RFX were predominantly upregulated (Figures S5C–S5G). Thus, FK228 is capable of upregulating subsets of genes that are expressed at reduced levels in the ears of *Rest*^{+/-ΔEx4} mice.

The fact that FK228 alters the expression of many genes that are unaffected in *Rest*^{+/-ΔEx4} mice raised the possibility that the observed rescue of *Rest*^{+/-ΔEx4} OHCs could result from a block in a general cell death pathway. To test this possibility, we added FK228 to organ of Corti cultures derived from newborn *Gfi1*^{-/-} mice, whose IHCs (like the OHCs of *Rest*^{+/-ΔEx4} mice) are subject to post-natal apoptotic cell death (Wallis et al., 2003). F-actin staining of organ of Corti cultures incubated with FK228 demonstrated that this inhibitor did not rescue the IHCs of *Gfi1*^{-/-} mice (Figure S6A). Thus, the ability of FK228 to rescue hair cells from degeneration depends on the specific molecular cause of the hair cell defect.

SAHA Rescues Hair Cells and Hearing in Rest Exon 4-Deficient Mice

HDAC inhibitors have not been examined for their abilities to cross the blood-perilymph barrier (BPB); however, a few have been studied for their ability to penetrate the BPB-like blood-brain barrier (BBB). These studies have shown that, although SAHA has a low brain-to-plasma ratio, it is more effective at crossing the BBB than other commercially available HDAC inhibitors (Hanson et al., 2013). Thus, we tested SAHA for the ability to rescue the OHCs of *Rest*^{+/-ΔEx4} mice *in vivo*, injecting mice subcutaneously with SAHA or vehicle (solvent) at P2, P4, and P5. F-actin staining of the organ of Corti of vehicle-injected *Rest*^{+/-ΔEx4} mice revealed that most OHCs lacked stereocilia at P6. In contrast, in the SAHA-injected *Rest*^{+/-ΔEx4} mice, most OHCs retained these structures (Figures 6C, 6D, and S6B). Thus, the OHCs of *Rest*^{+/-ΔEx4} mice can be rescued *in vivo* by systemically administered SAHA.

Given that in *Rest*^{+/-ΔEx4} mice the IHCs had degenerated by the time of SAHA injection, we tested IHC survival in organs of Corti that were exposed to HDAC inhibitors from the time of deletion of *Rest* exon 4. Organ of Corti cultures from P5 WT and *Rest*^{+/-ΔEx4}; *Rosa*^{+CreERT2} mice were incubated with tamoxifen or solvent at DIV3 and DIV4 (Figure 6E). A subset of these cultures was also incubated with FK228 or SAHA from DIV3 to DIV11. F-actin staining of these cultures at DIV12 demonstrated that SAHA and FK228 prevented the tamoxifen-dependent degeneration of IHCs and OHCs of *Rest*^{+/-ΔEx4}; *Rosa*^{+CreERT2} mice (Figures 6E and S6D). PCR analysis of the same cultures confirmed that tamoxifen induced recombination of loxP sites in nearly all copies of the *Rest*^{+/-ΔEx4} allele, independent of whether an HDAC inhibitor was present (Figure S6C). Thus, both IHCs and OHCs in *Rest* exon 4-deficient organ of Corti cultures can be rescued by exposure to HDAC inhibitors.

We assessed the effects of SAHA on the hearing of mice in which exon 4 was deleted post-natally. *Rest*^{+/-ΔEx4}; *Rosa*^{+CreERT2} and WT mice were injected subcutaneously with tamoxifen or vehicle from P7 to P9 and also with SAHA or vehicle daily from P7 to P15 (Figure 6F). At P16, hearing was tested using pure-tone stimuli and ABR recordings. The ABR analysis revealed that SAHA reduced the tamoxifen-dependent shift in hearing

threshold of *Rest*^{+/-ΔEx4}; *Rosa*^{+CreERT2} mice at low sound frequencies (Figure 6G). Histological analysis of cochleas of the same mice demonstrated that SAHA reduced the extent of tamoxifen-dependent hair cell loss (Figures 6F and S6E). In WT mice, tamoxifen affected neither hearing nor the survival of hair cells. Thus, SAHA alleviated the cochlear defects associated with the deletion of *Rest* exon 4.

Given that SAHA was more effective in rescuing the OHCs of *Rest* exon 4-deficient mice at P6 than P16 (Figures 6D and 6F), we tested the effects of SAHA injection on acetylation of histone H4 in OHCs at P6 and P16. Immunofluorescence analysis showed that SAHA injection led to an increase in H4 acetylation at both time points; however, at P6 the magnitude of the increase was ~6-fold larger than at P16 (Figure S6F). In rodents the BPB develops between P4 and P14 (Suzuki et al., 1998), and thus hair cells may be more accessible to systemically delivered SAHA at P6 than P16.

DISCUSSION

Here we identify *REST* as a novel deafness gene in humans, and we show that the deafness-causing variant prevents inactivation of the REST protein by alternative splicing. We also show that a mouse model of the *REST* splicing defect is characterized by deafness and degeneration of mechanosensory hair cells, and we demonstrate that both hair cells and hearing can be partially rescued in these mice by applying the HDAC inhibitor SAHA. Overall, our data indicate that alternative splicing is critical for REST inactivation in hair cells and that defects in this mechanism can be offset by chemical inhibition of HDACs.

Although mutations in the constitutively spliced exons of *REST* have been linked to cancer and gingival fibromatosis (Mahamadallie et al., 2015; Bayram et al., 2017), ours is the first study to associate REST with hearing loss, and *DFNA27* is the first genetic variant shown to affect the alternative splicing of REST. The effects of the *DFNA27* variant are highly unusual in that either gain or loss of function of the encoded protein occurs depending on the cellular context. In cells expressing the splicing factor SRRM4, the variant prevents REST inactivation by alternative splicing (gain of function), whereas in cells lacking SRRM4 it causes REST inactivation (loss of function). Our study suggests that the gain-of-function effect of *DFNA27* is deafness causing because selective prevention of alternative splicing-dependent inactivation of mouse REST also leads to deafness (Figure 1). In addition, in mice heterozygous for deletion of the first coding exon of *Rest* (*Rest*^{+/-}), the hearing threshold is similar to those of WT littermates, at least until P130 (Figure S3K). Thus, heterozygosity for loss-of-function mutations in *REST* may not impair hearing in humans.

Our results provide a plausible explanation for an apparent discrepancy: *DFNA27*-associated hearing loss is postlingual and progressive, yet *Rest*^{+/-ΔEx4} mice are deaf by the time of normal hearing onset (i.e., P12–P16). Specifically, our results indicate that, whereas the mouse *Rest*^{ΔEx4} mutation completely prevents exon 4-dependent inactivation of the encoded protein, the human *DFNA27* variant prevents exon 4b-dependent inactivation of REST without inhibiting exon 4a-dependent truncation of the encoded protein.

Our data shed new light on *Srrm4* regulation in the ear. Although *Srrm4* is repressed by REST in several cell types (Raj et al., 2011), in the hair cells of *Rest^{+/ΔEx4}* mice increased REST activity is not associated with reduced *Srrm4* expression. Given that the *Srrm4* promoter contains binding sites for the transcription factor ATOH1 and its binding dramatically induces *Srrm4* expression in hair cells (Cai et al., 2015), we speculate that in developing hair cells ATOH1 predominates over REST in regulating *Srrm4*.

Our findings also have implications for the cause of the inner ear defects in the Bronx waltzer (*bv*) mouse line. In this line, an *Srrm4*-truncating mutation (*Srrm4^{bv/bv}*) is associated with degeneration of most hair cells, as well as impaired hearing and balance (Nakano et al., 2012). In the balance organs of *Srrm4^{bv/bv}* mice, the incorporation of *Rest* exon 4, as well as that of alternative exons of ~50 other genes, is abnormally inefficient. Based on our current analysis, we speculate that the reduced incorporation of *Rest* exon 4 is one of multiple causes of the degeneration of hair cells in *Srrm4^{bv/bv}* mice.

RNA-seq analysis of utricles of *Rest^{+/ΔEx4}* mice revealed reduced expression of over 20 genes that are required for hearing and/or balance. Given that none of the previously characterized mutations in these genes is associated with hair cell loss of the same severity as the *Rest^{ΔEx4}* mutation, the hair cell degeneration observed in *Rest^{+/ΔEx4}* mice is unlikely to be caused by reduced expression of a single characterized gene. Thus, we speculate that reduced expression of multiple genes contributes to the hair cell defect in *Rest^{+/ΔEx4}* mice. Our RNA-seq data also indicate that alternative splicing of REST affects both the neuronal and non-neuronal sectors of the hair cell transcriptome. Nearly half of the genes expressed at reduced levels in the *Rest^{+/ΔEx4}* utricle are either high-confidence REST targets or potential RFX targets. Whereas most of high-confidence REST targets are transcribed selectively in neurons and hair cells, many of the potential RFX target genes encode kinocilium-related proteins that are not expressed in neurons. Given that nearly all of these kinocilium-related genes lack high-confidence binding sites for REST and are co-expressed with *Rest* in multi-ciliated epithelia, we suggest that the effect of REST on these genes in hair cells is indirect and cell type specific.

DFNA27 is the first example of a non-syndromic, deafness-causing gene defect whose consequences can be ameliorated in a model organism by applying SAHA, an FDA-approved compound for the treatment of cutaneous T cell lymphomas (Mann et al., 2007); however, many other HDAC inhibitors have been developed. Some of those that were developed most recently and are not yet commercialized have better tissue penetration and HDAC1 and HDAC2 selectivity than SAHA (Wagner et al., 2015). We suggest that these compounds hold promise for providing therapeutic benefits in cases of progressive hearing loss caused by gain-of-function mutations in *REST*.

STAR★METHODS

Detailed methods are provided in the online version of this paper and include the following:

- KEY RESOURCES TABLE
- CONTACT FOR REAGENT AND RESOURCE SHARING

● EXPERIMENTAL MODEL AND SUBJECT DETAILS

- Human Subjects
- Mice
- Generation of *Rest^{+/ΔEx4}* Mice
- Cell Lines and Tissue Culture

● METHOD DETAILS

- Hearing and Balance Tests
- Isolation and Analyses of DNA and RNA
- Immunofluorescence and Histochemistry
- Single Cell RT-PCR
- Cloning Procedures
- Splicing Assays in Transfected Cells
- qRT-PCR Analysis of HDAC Inhibitor-Incubated Cells
- Reporter Gene-Based Assays and Immunoblotting
- Incubation of Organ of Corti Cultures with HDAC Inhibitors
- RNA Sequencing and Bioinformatics Analyses
- SAHA Treatment of Mice

● QUANTIFICATION AND STATISTICAL ANALYSIS

● DATA AND SOFTWARE AVAILABILITY

SUPPLEMENTAL INFORMATION

Supplemental Information includes six figures and six tables and can be found with this article online at <https://doi.org/10.1016/j.cell.2018.06.004>.

ACKNOWLEDGMENTS

We thank the LMG2 family for participation in this study. We thank Susan Wiechert for technical assistance; Jian Zuo for providing the *Gfi1^{+/Cre}* mouse; Dennis Drayna, Doris Wu, and Christine Blaumueller for critical review of the manuscript; and Stephen Elledge for providing REST-encoding plasmids. This project was supported by grants from NIDCD/NIH (R01DC010152 and R01DC014953 to B.B.) and in part by funds from the NIDCD Division of Intramural Research/NIH (DC000048 to T.B.F., DC000086 to R.J.M., and DC000059 to M.W.K.). This work utilized computational resources of the NIH HPC Biowulf cluster (<https://hpc.nih.gov>).

AUTHOR CONTRIBUTIONS

B.B., T.B.F., M.W.K., and Y.N. designed the study. R.J.M., T.B.F., and A.U.R. analyzed data from human subjects. M.C.K. performed single-cell experiments. E.T.B., R.J.M., and B.B. performed the RNA-seq analyses. Y.N. performed all other experiments. All authors contributed to writing the manuscript.

DECLARATION OF INTERESTS

The authors declare no competing interests.

Received: June 30, 2017

Revised: March 11, 2018

Accepted: May 31, 2018

Published: June 28, 2018

REFERENCES

- Ballas, N., Grunseich, C., Lu, D.D., Speh, J.C., and Mandel, G. (2005). REST and its corepressors mediate plasticity of neuronal gene chromatin throughout neurogenesis. *Cell* 121, 645–657.
- Bayram, Y., White, J.J., Elcioglu, N., Cho, M.T., Zadeh, N., Gedikbasi, A., Palanduz, S., Ozturk, S., Cefle, K., Kasapcopur, O., et al.; Baylor-Hopkins Center for Mendelian Genomics (2017). REST final-exon-truncating mutations cause hereditary gingival fibromatosis. *Am. J. Hum. Genet.* 101, 149–156.

- Burns, J.C., Kelly, M.C., Hoa, M., Morell, R.J., and Kelley, M.W. (2015). Single-cell RNA-Seq resolves cellular complexity in sensory organs from the neonatal inner ear. *Nat. Commun.* 6, 8557.
- Cai, T., Jen, H.I., Kang, H., Kirsch, T.J., Zoghbi, H.Y., and Groves, A.K. (2015). Characterization of the transcriptome of nascent hair cells and identification of direct targets of the Atoh1 transcription factor. *J. Neurosci.* 35, 5870–5883.
- Calarco, J.A., Superina, S., O'Hanlon, D., Gabut, M., Raj, B., Pan, Q., Skalska, U., Clarke, L., Gelinis, D., van der Kooy, D., et al. (2009). Regulation of vertebrate nervous system alternative splicing and development by an SR-related protein. *Cell* 138, 898–910.
- Chen, Z.F., Paquette, A.J., and Anderson, D.J. (1998). NRSF/REST is required in vivo for repression of multiple neuronal target genes during embryogenesis. *Nat. Genet.* 20, 136–142.
- Chong, J.A., Tapia-Ramírez, J., Kim, S., Toledo-Aral, J.J., Zheng, Y., Boutros, M.C., Altshuller, Y.M., Frohman, M.A., Kraner, S.D., and Mandel, G. (1995). REST: a mammalian silencer protein that restricts sodium channel gene expression to neurons. *Cell* 80, 949–957.
- Dobin, A., Davis, C.A., Schlesinger, F., Drenkow, J., Zaleski, C., Jha, S., Batut, P., Chaisson, M., and Gingeras, T.R. (2013). STAR: ultrafast universal RNA-seq aligner. *Bioinformatics* 29, 15–21.
- ENCODE Project Consortium (2012). An integrated encyclopedia of DNA elements in the human genome. *Nature* 489, 57–74.
- Farley, F.W., Soriano, P., Steffen, L.S., and Dymecki, S.M. (2000). Widespread recombinase expression using FLPeR (flipper) mice. *Genesis* 28, 106–110.
- Ganesan, A. (2015). Macroyclic inhibitors of zinc-dependent histone deacetylases (HDACs). In *Macrocycles in Drug Discovery*, J. Levin, ed. (Royal Society of Chemistry), pp. 109–140.
- Gao, Z., Ure, K., Ding, P., Nashaat, M., Yuan, L., Ma, J., Hammer, R.E., and Hsieh, J. (2011). The master negative regulator REST/NRSF controls adult neurogenesis by restraining the neurogenic program in quiescent stem cells. *J. Neurosci.* 31, 9772–9786.
- Gong, S., Zheng, C., Doughty, M.L., Losos, K., Didkovsky, N., Schambra, U.B., Nowak, N.J., Joyner, A., Leblanc, G., Hatten, M.E., and Heintz, N. (2003). A gene expression atlas of the central nervous system based on bacterial artificial chromosomes. *Nature* 425, 917–925.
- Hameyer, D., Loonstra, A., Eshkind, L., Schmitt, S., Antunes, C., Groen, A., Bindels, E., Jonkers, J., Krimpenfort, P., Meuwissen, R., et al. (2007). Toxicity of ligand-dependent Cre recombinases and generation of a conditional Cre deleter mouse allowing mosaic recombination in peripheral tissues. *Physiol. Genomics* 31, 32–41.
- Hanson, J.E., La, H., Plise, E., Chen, Y.H., Ding, X., Hanania, T., Sabath, E.V., Alexandrov, V., Brunner, D., Leahy, E., et al. (2013). SAHA enhances synaptic function and plasticity in vitro but has limited brain availability in vivo and does not impact cognition. *PLoS ONE* 8, e69964.
- Hartley, S.W., and Mullikin, J.C. (2016). Detection and visualization of differential splicing in RNA-Seq data with JunctionSeq. *Nucleic Acids Res.* 44, e127.
- Huang da, W., Sherman, B.T., and Lempicki, R.A. (2009). Systematic and integrative analysis of large gene lists using DAVID bioinformatics resources. *Nat. Protoc.* 4, 44–57.
- Karolchik, D., Hinrichs, A.S., Furey, T.S., Roskin, K.M., Sugnet, C.W., Haussler, D., and Kent, W.J. (2004). The UCSC Table Browser data retrieval tool. *Nucleic Acids Res.* 32, D493–D496.
- Khan, A., Fornes, O., Stigliani, A., Gheorghe, M., Castro-Mondragon, J.A., van der Lee, R., Bessy, A., Chèneby, J., Kulkarni, S.R., Tan, G., et al. (2018). JASPAR 2018: update of the open-access database of transcription factor binding profiles and its web framework. *Nucleic Acids Res.* 46 (D1), D260–D266.
- Konsoula, R., and Jung, M. (2008). In vitro plasma stability, permeability and solubility of mercaptoacetamide histone deacetylase inhibitors. *Int. J. Pharm.* 361, 19–25.
- Lewandoski, M., Meyers, E.N., and Martin, G.R. (1997). Analysis of Fgf8 gene function in vertebrate development. *Cold Spring Harb. Symp. Quant. Biol.* 62, 159–168.
- Love, M.I., Huber, W., and Anders, S. (2014). Moderated estimation of fold change and dispersion for RNA-seq data with DESeq2. *Genome Biol.* 15, 550.
- Magin, A., Lietz, M., Cibelli, G., and Thiel, G. (2002). RE-1 silencing transcription factor-4 (REST4) is neither a transcriptional repressor nor a de-repressor. *Neurochem. Int.* 40, 195–202.
- Mahamdallie, S.S., Hanks, S., Karlin, K.L., Zachariou, A., Perdeaux, E.R., Ruark, E., Shaw, C.A., Renwick, A., Ramsay, E., Yost, S., et al. (2015). Mutations in the transcriptional repressor REST predispose to Wilms tumor. *Nat. Genet.* 47, 1471–1474.
- Mandel, G., Fiondella, C.G., Covey, M.V., Lu, D.D., Loturco, J.J., and Ballas, N. (2011). Repressor element 1 silencing transcription factor (REST) controls radial migration and temporal neuronal specification during neocortical development. *Proc. Natl. Acad. Sci. USA* 108, 16789–16794.
- Mann, B.S., Johnson, J.R., Cohen, M.H., Justice, R., and Pazdur, R. (2007). FDA approval summary: vorinostat for treatment of advanced primary cutaneous T-cell lymphoma. *Oncologist* 12, 1247–1252.
- Manojlovic, Z., Earwood, R., Kato, A., Stefanovic, B., and Kato, Y. (2014). RFX7 is required for the formation of cilia in the neural tube. *Mech. Dev.* 132, 28–37.
- McGann, J.C., Oyer, J.A., Garg, S., Yao, H., Liu, J., Feng, X., Liao, L., Yates, J.R., 3rd, and Mandel, G. (2014). Polycomb- and REST-associated histone deacetylases are independent pathways toward a mature neuronal phenotype. *eLife* 3, e04235.
- Method, J.L., Chakravarty, P.K., Chenard, M., Close, J., Cruz, J.C., Dahlberg, W.K., Fleming, J., Hamblett, C.L., Hamill, J.E., Harrington, P., et al. (2008). Exploration of the internal cavity of histone deacetylase (HDAC) with selective HDAC1/HDAC2 inhibitors (SHI-1:2). *Bioorg. Med. Chem. Lett.* 18, 973–978.
- Nakano, Y., Jahan, I., Bonde, G., Sun, X., Hildebrand, M.S., Engelhardt, J.F., Smith, R.J., Cornell, R.A., Fritzsch, B., and Bánfi, B. (2012). A mutation in the Srrm4 gene causes alternative splicing defects and deafness in the Bronx waltzer mouse. *PLoS Genet.* 8, e1002966.
- Nechiporuk, T., McGann, J., Mullendorff, K., Hsieh, J., Wurst, W., Floss, T., and Mandel, G. (2016). The REST remodeling complex protects genomic integrity during embryonic neurogenesis. *eLife* 5, e09584.
- Palm, K., Metsis, M., and Timmus, T. (1999). Neuron-specific splicing of zinc finger transcription factor REST/NRSF/XBR is frequent in neuroblastomas and conserved in human, mouse and rat. *Brain Res. Mol. Brain Res.* 72, 30–39.
- Paquette, A.J., Perez, S.E., and Anderson, D.J. (2000). Constitutive expression of the neuron-restrictive silencer factor (NRSF)/REST in differentiating neurons disrupts neuronal gene expression and causes axon pathfinding errors in vivo. *Proc. Natl. Acad. Sci. USA* 97, 12318–12323.
- Peters, L.M., Fridell, R.A., Boger, E.T., San Agustin, T.B., Madeo, A.C., Griffith, A.J., Friedman, T.B., and Morell, R.J. (2008). A locus for autosomal dominant progressive non-syndromic hearing loss, DFNA27, is on chromosome 4q12-13.1. *Clin. Genet.* 73, 367–372.
- Raj, B., O'Hanlon, D., Vessey, J.P., Pan, Q., Ray, D., Buckley, N.J., Miller, F.D., and Blencowe, B.J. (2011). Cross-regulation between an alternative splicing activator and a transcription repressor controls neurogenesis. *Mol. Cell* 43, 843–850.
- Raj, B., Irimia, M., Braunschweig, U., Sterne-Weiler, T., O'Hanlon, D., Lin, Z.Y., Chen, G.I., Easton, L.E., Ule, J., Gingras, A.C., et al. (2014). A global regulatory mechanism for activating an exon network required for neurogenesis. *Mol. Cell* 56, 90–103.
- Scheffer, D.I., Shen, J., Corey, D.P., and Chen, Z.Y. (2015). Gene expression by mouse inner ear hair cells during development. *J. Neurosci.* 35, 6366–6380.
- Schoenher, C.J., and Anderson, D.J. (1995). The neuron-restrictive silencer factor (NRSF): a coordinate repressor of multiple neuron-specific genes. *Science* 267, 1360–1363.
- Suzuki, M., Yamasoba, T., and Kaga, K. (1998). Development of the blood-labyrinth barrier in the rat. *Hear. Res.* 116, 107–112.
- Wagner, F.F., Zhang, Y.L., Fass, D.M., Joseph, N., Gale, J.P., Weiwer, M., McCarron, P., Fisher, S.L., Kaya, T., Zhao, W.N., et al. (2015). Kinetically

selective inhibitors of histone deacetylase 2 (HDAC2) as cognition enhancers. *Chem. Sci. (Camb.)* 6, 804–815.

Wallis, D., Hamblen, M., Zhou, Y., Venken, K.J., Schumacher, A., Grimes, H.L., Zoghbi, H.Y., Orkin, S.H., and Bellen, H.J. (2003). The zinc finger transcription factor Gfi1, implicated in lymphomagenesis, is required for inner ear hair cell differentiation and survival. *Development* 130, 221–232.

Westbrook, T.F., Hu, G., Ang, X.L., Mulligan, P., Pavlova, N.N., Liang, A., Leng, Y., Maehr, R., Shi, Y., Harper, J.W., and Elledge, S.J. (2008). SCF β -TRCP controls oncogenic transformation and neural differentiation through REST degradation. *Nature* 452, 370–374.

Yang, H., Gan, J., Xie, X., Deng, M., Feng, L., Chen, X., Gao, Z., and Gan, L. (2010). Gfi1-Cre knock-in mouse line: A tool for inner ear hair cell-specific gene deletion. *Genesis* 48, 400–406.

STAR★METHODS

KEY RESOURCES TABLE

REAGENT or RESOURCE	SOURCE	IDENTIFIER
Antibodies		
Mouse anti-Acetylated Tubulin monoclonal antibody (clone 6-11B-1)	Sigma	Cat# T7451; RRID: AB_609894
Rabbit anti-MYO7A antibody	Proteus Biosciences	Cat# 25-6790; RRID: AB_10015251
Mouse anti- MYO7A antibody	University of Iowa Developmental Studies Hybridoma Bank	Cat# Myo7A 138-1; RRID:AB_2282417
Rabbit anti-H4ac antibody	Active Motif	Cat# 39244; RRID: AB_2687872
Rabbit anti-GFP antibody	Novus	NB600-308; RRID: AB_10003058
Mouse anti-SATB2 monoclonal antibody (clone SATBA4B10)	Santa Cruz	Cat# sc-81376; RRID: AB_882455
Rabbit anti-TBR1 antibody	Abcam	Cat# ab31940; RRID: AB_2200219
Mouse anti-NeuN monoclonal antibody (clone A60)	Millipore	Cat# MAB377; RRID: AB_2298772
Rabbit anti-PAX6 antibody	Biolegend	Cat# 901301; RRID: AB_2565003
Goat anti-TAG1 antibody	R&D Systems	Cat# AF4439; RRID: AB_2044647
Rabbit anti-cleaved CASP3 monoclonal antibody (clone D3E9)	Cell Signaling	Cat# 9579; RRID: AB_10897512
Mouse anti-FLAG monoclonal antibody (clone M2)	Sigma	Cat# F3165; RRID: AB_259529
Rabbit anti-LMNB1 antibody	Abcam	Cat# ab16048; RRID: AB_443298
Alexa 488-conjugated donkey anti-goat antibody	Thermo Fisher Scientific	Cat# A-11055; RRID: AB_253410
Alexa 488-conjugated donkey anti-mouse antibody	Thermo Fisher Scientific	Cat# A-21202; RRID: AB_141607
Alexa 594-conjugated donkey anti-rabbit antibody	Thermo Fisher Scientific	Cat# A-21207; RRID: AB_141637
Alexa 568-conjugated donkey anti-mouse antibody	Thermo Fisher Scientific	Cat# A10037; RRID: AB_2534013
Alexa 488-conjugated donkey anti-rabbit antibody	Thermo Fisher Scientific	Cat# A-21207; RRID: AB_2535792
Sheep AP-conjugated anti-digoxigenin antibody	Roche	Cat# 11093274910; RRID: AB_514497
HRP-conjugated donkey anti-rabbit antibody	GE Healthcare Life Science	Cat# NA934-1ML; RRID: AB_772206
HRP-conjugated goat anti-mouse antibody	Bio-Rad	Cat# 170-6516; RRID: AB_11125547
Biological Samples		
Human Fetal Brain Total RNA	Clontech	Cat# 636526
Human Spleen Total RNA	Clontech	Cat# 636525
Chemicals, Peptides, and Recombinant Proteins		
(Z)-4-hydroxytamoxifen	Tocris Bioscience	Cat# 3412
DIG DNA Labeling and Detection Kit	Roche	Cat# 11 093 657 910
Lipofectamine LTX Reagent with PLUS Reagent	Thermo Fisher Scientific	Cat# 15338100
Trizol Reagent	Thermo Fisher Scientific	Cat# 15596018
Alexa Fluor 488 Phalloidin	Thermo Fisher Scientific	Cat# A12379
Cremophor EL	Millipore	Cat# 238470
SAHA	Selleckchem.com	Cat# S1047
FK228	APExBIO	Cat# A8173
Merck60 4-(acetylamino)-N-[2-amino-5-(2-thienyl)phenyl]-benzamide	Otava Chemicals	N/A
Z-DEVD-FMK	R&D Systems	Cat# FMK004
Z-VAD-FMK	R&D Systems	Cat# FMK001
Thermolysin	Sigma	Cat# T7902
DNase I	STEMCELL Technologies	Cat# 07900
Papain	Worthington	Cat# LS003118

(Continued on next page)

Continued

REAGENT or RESOURCE	SOURCE	IDENTIFIER
SPRI Select Beads	Beckman Coulter	Cat# B23317
LongAmp DNA polymerase	New England BioLabs	Cat# M0323S
RNase-Free DNase Set	QIAGEN	Cat# 79254
TrypLE Select	Thermo Fisher Scientific	Cat# 12563011
Critical Commercial Assays		
SuperScript IV First-Strand Synthesis System	Thermo Fisher Scientific	Cat# 18091050
SuperScript III First-Strand Synthesis System	Thermo Fisher Scientific	Cat# 18080051
ThermoScript Reverse Transcriptase	Thermo Fisher Scientific	Cat# 12236-014
Dual-Luciferase Reporter Assay System	Promega	Cat# E1910
PAXgene Blood RNA Kit	QIAGEN	Cat# 762164
Agencourt AMPure XP System	Beckman Coulter	Cat# A63880
RNeasy Mini Kit	QIAGEN	Cat# 74104
RNeasy Micro Kit	QIAGEN	Cat# 74004
PicoPure DNA Extraction Kit	Thermo Fisher Scientific	Cat# KIT0103
High Sensitivity Large Fragment Analysis Kit	Advanced Analytical	Cat#: DNF-493
High Sensitivity NGS Fragment Analysis Kit	Advanced Analytical	Cat#: DNF-474
APEX Alexa Fluor 488 Antibody Labeling Kit	Thermo Fisher Scientific	Cat# A10468
APEX Alexa Fluor 568 Antibody Labeling Kit	Thermo Fisher Scientific	Cat# A10494
Nextera XT Library Prep Kit	Illumina	Cat# FC-131-1024
Deposited Data		
RNA-seq data (utricle)	This paper	GEO: GSE111606
RNA-seq data (brain cortex)	This paper	GEO: GSE111606
RNA-seq data (organ of Corti cultures exposed to FK228 or solvent)	This paper	GEO: GSE111606
Experimental Models: Cell Lines		
HEK293 cells	ATCC	Cat# CRL-1573
Neuro2a cells	ATCC	Cat# CCL-131
Experimental Models: Organisms/Strains		
Mouse: B6.129S6- <i>Rest</i> ^{+/ΔEx4}	This paper	N/A
Mouse: wild type C57BL/6J	Charles River Laboratories	Cat# 027
Mouse: <i>Tg(Rest-EGFP)DG302Gsat/Mmucl</i> (SWR/J)	MMRRC Repository	Cat# 011583-UCD
Mouse: B6.129S6(Cg)- <i>Rest</i> ^{tm1.1Jhsj} /J	The Jackson Laboratory	Cat# 024549
Mouse: FVB/N- <i>Tmem163</i> ^{Tg(ACTB-cre)2Mrt} /J	The Jackson Laboratory	Cat# 003376
Mouse: B6.129-Gt(ROSA)26Sor ^{tm1(cre/ERT2)Tyr} /J	The Jackson Laboratory	Cat# 008463
Mouse: 129S4/SvJaeSor-Gt(ROSA)26Sor ^{tm1(FLP1)Dym} /J	The Jackson Laboratory	Cat# 003946
Mouse: CD-1	Charles River Laboratories	Cat# 022
Mouse: B6.Cg-Gt(ROSA)26Sor ^{tm1(CAG-tdTomato)Hze} /J	The Jackson Laboratory	Cat# 007914
Mouse: FVB/N- <i>Gf1</i> ^{+/-Cre}	Yang et al., 2010	N/A
Oligonucleotides		
List of primers and synthetic gene fragments	Table S6	N/A
Recombinant DNA		
Exontrap Cloning Vector pET01	MoBiTec	Cat# pET01
<i>REST</i> ^{WT} -pET01 minigene	This paper	N/A
<i>REST</i> ^{DNA27} -pET01 minigene	This paper	N/A
LPC-flag- <i>REST</i> ^Δ	Westbrook et al., 2008	Addgene 41903
LPC-flag- <i>REST</i> ^{Δa}	This paper	N/A
LPC-flag- <i>REST</i> ^{ΔaM}	This paper	N/A

(Continued on next page)

Continued

REAGENT or RESOURCE	SOURCE	IDENTIFIER
LPC-flag- <i>REST</i> ^{4b}	This paper	N/A
LPC-flag- <i>REST</i> ^{4bM}	This paper	N/A
pGL4.10[luc2]	Promega	Cat# E6651
pGL4.74[hRluc/TK]	Promega	Cat# E6921
RE1-TK-pGL4.10[luc2]	This paper	N/A
TK-pGL4.10[luc2]	This paper	N/A
TK- <i>Rfx7</i> -RE1L-pGL4.10[luc2]	This paper	N/A
TK- <i>Rfx7</i> -RE1L ^{MUT} -pGL4.10[luc2]	This paper	N/A
<i>SRRM4</i> -pcDNA3.1+	This paper	N/A
BAC clone RP23-27L14	Children's Hospital Oakland Research Institute	RP23-27L14
Software and Algorithms		
ImageJ2	NIH	https://imagej.net/ImageJ2 RRID: SCR_003070
Zen lite 2012	Zeiss	https://www.zeiss.com/microscopy/us/products/microscope-software/zen.html RRID: SCR_013672
GraphPad PRISM v.7.00	GraphPad Prism	https://www.graphpad.com/scientific-software/prism/ RRID: SCR_002798
SINGuLAR Analysis Toolset software v3.6.2	Fluidigm	https://www.fluidigm.com/software
R 3.0.2	CRAN R project	https://cran.r-project.org/ RRID: SCR_001905
STAR aligner v2.5.2a	Dobin et al., 2013	https://github.com/alexdobin/STAR
DESeq2 v.1.4.5	Love et al., 2014	https://github.com/mikelove/DESeq2 RRID: SCR_015687
UCSC Table Browser	Karolchik et al., 2004	https://genome.ucsc.edu/cgi-bin/hgTables
JunctionSeq v.1.5.4	Hartley and Mullikin, 2016	https://github.com/hartleys/JunctionSeq
Multiple Primer Analyzer	Thermo Fisher Scientific	https://www.thermofisher.com/us/en/home/brands/thermo-scientific/molecular-biology/molecular-biology-learning-center/molecular-biology-resource-library/thermo-scientific-web-tools/multiple-primer-analyzer.html
NCBI Primer-BLAST	NCBI - NIH	https://www.ncbi.nlm.nih.gov/tools/primer-blast/
DAVID	Huang da et al., 2009	https://david.ncifcrf.gov/ RRID: SCR_001881

CONTACT FOR REAGENT AND RESOURCE SHARING

Further information and requests for resources and reagents should be directed to and will be fulfilled by the Lead Contact, Botond Bánfi (botond-banfi@uiowa.edu).

EXPERIMENTAL MODEL AND SUBJECT DETAILS**Human Subjects**

All human subjects-related procedures were approved by the Combined Neuroscience Institutional Review Board at the National Institutes of Health (NIH), Bethesda, MD, USA. Written informed consent was obtained from all participants. Venous blood was collected from the study subjects for DNA and RNA isolations. The ages of subjects were between 14 and 72 at the time of blood collection. The number and gender of participating subjects are shown in Figure 2B. Audiometric data for the participating subjects were described previously (Peters et al., 2008).

Mice

All mouse procedures were approved by the University of Iowa Institutional Animal Care and Use Committee. Mice were housed in groups in temperature controlled rooms ($21 \pm 2^\circ\text{C}$) with 12 h/12 h light/dark cycle. Food and water were available for the mice *ad libitum*. Animal husbandry and health status monitoring were provided by the Office of Animal Resources staff at the University of Iowa. The ages of tested mice are indicated in the figure legends. The sexes of pre-weaning mice were not determined. The sexes of weaned mice (P21 and older) were documented. Male and female *Rest*^{+/-Ex4} mice exhibited equally severe hearing loss and

balance defect. The *Rest* promoter-EGFP transgenic mouse line was generated in the GENSAT project and made available through the Mutant Mouse Resource and Research Center (Gong et al., 2003). Heterozygous *Gfi1*^{+/Cre} and homozygous *Gfi1*^{Cre/Cre} mice were described previously (Yang et al., 2010). In the current study, *Gfi1*^{+/Cre} mice were used to express Cre selectively in hair cells within the inner ear. *Gfi1*^{Cre/Cre} mice were used for experiments shown in Figure S6A. In the *Gfi1*^{Cre} allele, the Cre-encoding sequence replaces the protein-coding region of *Gfi1*. We refer to the *Gfi1*^{Cre/Cre} mice as *Gfi1*^{-/-} to emphasize that the goal was the inactivation of both *Gfi1* alleles in Figure S6A as opposed to the expression of the Cre recombinase. *Rest*^{+/+} mice were generated by intercrossing the previously described *Rest* exon 2-floxed mouse line with the β -actin-Cre transgenic mouse line (Lewandoski et al., 1997; Gao et al., 2011).

Generation of *Rest*^{+/ΔEx4} Mice

Conventional gene targeting was used to insert loxP site upstream and downstream of exon 4 of *Rest* (*Rest*^{fl/flNeoEx4}) in mouse ES cells (Figure S1A). Two recombination-positive ES cell clones were selected for the production of *Rest*^{+/flNeoEx4} mice. Recombination of the targeting vector with the mouse genome was confirmed by PCR (see primers in Table S6) and Southern blotting, in both ES cells and *Rest*^{+/flNeoEx4} mice. For Southern blot analysis, genomic DNA was digested with the EcoRI, SpeI or BgIII restriction endonuclease (New England Biolabs). Electrophoretically separated digestion products were transferred to positively charged nylon membranes (Roche) and hybridized with digoxigenin-labeled probes. Three probes were designed: one from the neomycin-resistance gene (Neo) of the targeting construct, and two from genomic regions that flank the targeted segment of *Rest* (Figure S1A). Digoxigenin-labeled nucleotides were incorporated into the probes using the DIG DNA Labeling and Detection Kit (Roche). The same kit was also used for the visualization of hybridized probes, following the manufacturer's instructions. To remove Neo from the *Rest*^{fl/flNeoEx4} allele, *Rest*^{+/flNeoEx4} mice were bred with *Rosa*^{FLP1/FLP1} knock-in mice (Farley et al., 2000). Finally, the floxed exon was removed by intercrossing the *Rest*^{+/flEx4} mouse line with Cre-expressing mouse lines, including β -actin-Cre transgenic, *Gfi1*^{+/Cre} knock-in, and *Rosa*^{+/CreERT2} knock-in mice (Lewandoski et al., 1997; Hameyer et al., 2007; Yang et al., 2010). In *Rest*^{+/flEx4},*Rosa*^{+/CreERT2} mice, Cre recombinase activity was induced using one of two regimens of injections with (Z)-4-hydroxytamoxifen (Tocris Bioscience), depending on the age of the mice: P7–9 mice were subcutaneously injected with (Z)-4-hydroxytamoxifen (33 mg/kg body weight) daily for 3 days; P40–47 mice were intraperitoneally injected with (Z)-4-hydroxytamoxifen (33 mg/kg body weight) daily for 8 days.

Cell Lines and Tissue Culture

HEK293 cells (female) and Neuro2a cells (male) were obtained from the American Type Culture Collection (ATCC). HEK293 cells were grown in Dulbecco's Modified Eagle Medium/Nutrient Mixture F-12 (DMEM/F-12 from Corning). Neuro2a cells were grown in DMEM (Corning). Both DMEM/F12 and DMEM were supplemented with 10% fetal bovine serum (FBS from Atlanta Biologicals), penicillin (100 units/mL; Thermo Fisher Scientific), and streptomycin (100 μ g/mL; Thermo Fisher Scientific). Organs of Corti were dissected from P0–P5 mice and placed on Matrigel-coated transwell plates (Corning). The sexes of these mice were not determined. Organ cultures were maintained in neurobasal-A medium supplemented with B-27, N-2, 0.5 mM L-glutamine (all from Thermo Fisher Scientific), and 100 U/mL penicillin (Sigma). The culture medium was replaced on the organs once in every 3 days. Organ cultures and cell lines were grown at 37°C in the presence of 5% CO₂.

METHOD DETAILS

Hearing and Balance Tests

The ABR thresholds of mice were measured using a previously described open-field system, and both broadband and pure-tone stimuli (Nakano et al., 2012). The ability of mice to balance (P21–28) was evaluated by measuring the time each mouse could remain on a fixed horizontal rod (1.8 cm in diameter) following two training trials.

Isolation and Analyses of DNA and RNA

Genomic DNA was extracted from human blood samples as described previously (Peters et al., 2008). To analyze the *DFNA27* interval in the genomic DNA, two sets of PCR primers were designed. The first set was designed to amplify all annotated exons at the *DFNA27* locus and all conserved intronic segments in *REST*. The second set was designed specifically for the amplification of the exon 4-containing region of *REST* (see primers in Table S6). The PCR amplicons were Sanger sequenced using BigDye Terminator chemistry and an ABI3730 DNA Analyzer (Applied Biosystems). RNA was isolated from human blood samples using the PAX-gene Blood RNA Kit (QIAGEN), and was reverse transcribed using SuperScript III reverse transcriptase (Thermo Fisher Scientific). The cDNA products were analyzed for the presence of *REST* splice variants by PCR (see primers in Table S6). The PCR products were separated by size and sub-cloned into the pCR-TOPO vector (Thermo Fisher Scientific). A total of 180 clones were sequenced using the Sanger method. For the isolation of cortical RNA from mice, the neocortex was dissected from the brain and homogenized in Trizol Reagent (Thermo Fisher Scientific). RNA was extracted from the homogenized tissue with chloroform, and precipitated with isopropanol. RNA was dissolved in water, incubated with DNase, and further purified on the separation column of the RNeasy Mini Kit (QIAGEN), following the manufacturer's instructions. RNA was isolated from vestibular maculas and HEK293 cells using either the RNeasy Micro or Mini Kit (QIAGEN), depending on the number of cells in the samples. RNA samples from mice and HEK293 cells were reverse transcribed using SuperScript IV reverse transcriptase (Thermo Fisher Scientific). Human spleen RNA and fetal brain

RNA were purchased from Clontech Laboratories, and were reverse transcribed using either SuperScript IV or ThermoScript (Thermo Fisher Scientific). The ratio of the detected splice forms of *REST* was not affected by the choice of reverse transcriptase (data not shown). The cDNA samples produced were analyzed by PCR and qPCR (see primers in [Table S6](#)). PCR products less than 200 bp in length were separated in polyacrylamide gels; larger PCR products were separated in agarose gels.

Immunofluorescence and Histochemistry

The antibodies used for this study are listed in the [Key Resources Table](#). Whole-mount preparations of cochlear and vestibular tissues were fixed with 4% paraformaldehyde in PBS (4% PFA), and labeled with an anti-MYO7A antibody, an anti-H4ac antibody, an anti-acetylated- α -tubulin antibody, an anti-cleaved CASP3 antibody, or phalloidin-Alexa 488. The binding of primary antibodies to the specimens was tested using Alexa 488-conjugated, Alexa 568-conjugated, or Alexa 594-conjugated secondary antibodies. *Rest* promoter activity was examined in cortical and inner ear tissues using *Rest* promoter-EGFP transgenic mice. These mice were transcardially perfused with 4% PFA while under deep anesthesia. Inner ears and brains were dissected from the perfused mice, cryoprotected in sucrose solutions, embedded into Tissue Freezing Medium (Electron Microscopy Sciences), and cryosectioned. Sections were incubated with Alexa 488-conjugated anti-GFP antibody in combination with an Alexa 568-conjugated anti-MYO7A antibody or an Alexa 568-conjugated anti-NeuN antibody. The specificity of GFP detection was confirmed by probing inner ear and brain sections of WT mice with the Alexa 488-conjugated anti-GFP antibody. The APEX Antibody Labeling Kit (Thermo Fisher Scientific) was used for the conjugation of Alexa dyes to the antibodies. Layering of the neocortex was examined in P0 mice. Brain samples were fixed with 4% PFA, cryoprotected in sucrose solution, and embedded into Tissue Freezing Medium (Electron Microscopy Sciences). Cryosections were co-labeled with a mouse anti-SATB2 antibody and a rabbit anti-TBR1 antibody, or a mouse anti-NeuN antibody and a rabbit anti-PAX6 antibody. The binding of primary antibody was visualized with Alexa 488- and Alexa 594-conjugated secondary antibodies. For the labeling of commissural axons, mouse embryos (E11.5) were fixed with Prefer (Anatech) and processed for cryosectioning as described for the brain samples. Transverse sections of the rostral region of the spinal cord were probed with an anti-TAG1 antibody and an Alexa 488-conjugated secondary antibody. Images of fluorescently labeled tissues were acquired using an LSM 880 confocal microscope (Carl Zeiss) and analyzed using the ZEN lite 2012 software (Carl Zeiss) or ImageJ. For histochemical analysis of the brain, mice were transcardially perfused with 4% PFA while under deep anesthesia, after which the brain was dissected from the skull, embedded into paraffin, sectioned, and stained with H&E.

Single Cell RT-PCR

Cochleas were dissected from either CD-1 or *Gfi1*^{+/Cre},*Rosa*^{+/CAG-tdTomato} knock-in mice at P1 and P7 (the sexes of these mice were not determined). The organ of Corti-containing regions were dissected from the cochlea in ice-cold DMEM/F-12, and epithelia were removed from underlying mesenchyme following a 10-min treatment with 0.2 mg/mL thermolysin (Sigma) and 1.67 μ g/mL DNase I (Stem Cell Technologies) at 37°C. Cochlear epithelial sheets containing hair cells, supporting cells, and some surrounding non-sensory cells were dissociated by 15 min digestion with TrypLE Select (GIBCO) or papain (Worthington) at 37°C and by trituration at 5-min intervals during the digestion. Enzymatic digestions were quenched with an equal volume of ice-cold DMEM/F-12 containing 10% FBS, and nuclei were stained with 1 μ g/mL Hoechst 33342 (Thermo Fisher Scientific). Dissociated cells were pelleted and re-suspended in the volume of DMEM/F-12 necessary to achieve a cell concentration of ~500 cells/ μ L. cDNA was prepared from individual cells, and specific targets were pre-amplified using the Fluidigm C1 platform and either small (5–10 μ m) or medium-sized (10–17 μ m) integrated fluidic chips (Fluidigm), following the manufacturer's instructions. All capture sites of the integrated fluidic chips were imaged prior to cell lysis to identify the wells that contained viable single cells. Initial captures with non-transgenic mice were stained with 4 μ M Calcein AM dye (Thermo Fisher Scientific), to confirm cell viability based on esterase activity in the cytoplasm. Primers for pre-amplification and qPCR were designed with the NCBI Primer-BLAST tool or adopted from a previous study ([Burns et al., 2015](#)). Primer combinations were checked for multiplex primer dimerization using the Multiple Primer Analyzer Tool (Thermo Fisher Scientific). Single-cell cDNA samples were analyzed by qPCR on the Fluidigm BioMark HD platform (see primers in [Table S6](#)). The limit of detection (LOD) was set to Ct value 24, and expression data are reported as Log2 expression (Log2Ex) = LOD – Ct. qPCR assays were validated using a mouse universal cDNA library and a P1 mouse cochlear cDNA library, as described previously ([Burns et al., 2015](#)). Assay efficiencies were calculated as $10^{(-1/\text{slope})} - 1$ using a three-fold dilution series of pre-amplified cDNA. All assays used in this study had efficiencies between 0.926 and 1.124. Based on the expression data, cell IDs were grouped using unsupervised hierarchical clustering function of the SINGuLAR Analysis Toolset (Fluidigm) in R 3.0.2. The hair-cell representing cluster was identified based on the high average Log2Ex of 10 hair cell-specific transcripts (i.e., *Chgb*, *Gfi1*, *Myo15*, *Pvalb*, *Scg3*, *Scn3b*, *Snap25*, *Srrm3*, *Srrm4*, and *Myo7a*) across the cells ([Scheffer et al., 2015](#)). The 'non-hair cell' representing cluster was identified based on the low average expression of the 10 genes. In the hair-cell cluster, IHCs were identified based on the expression of *Fgf8* (Log2Ex > 6) and the lack of expression of *Slc26a5* (Log2Ex = 0). OHCs were identified based on the expression of *Slc26a5* (Log2Ex > 4 at P1 and Log2Ex > 10 at P7) and the lack of expression of *Fgf8* (Log2Ex = 0). Cells in which both *Fgf8* and *Slc26a5* were detected were excluded from analysis.

Cloning Procedures

The *Rest* exon 4-targeting construct was assembled in the pBlueScript vector. The left arm, floxed region, and right arm of the targeting construct was amplified by PCR using the mouse BAC clone RP23-27L14 (Children's Hospital Oakland Research Institute)

as template. Restriction sites were incorporated into the amplified DNA segments via PCR primers (Table S6). The Neo cassette was obtained from GeneBridges. The completed targeting construct was excised from pBlueScript by restriction digestion, and ES cells were electroporated with it. *REST* minigenes were generated by subcloning PCR-amplified exon 4 and its flanking introns (~350 bp in both directions), from a control subject and a DFNA27 subject, between two constitutively spliced exons in the pET-01 vector (Mobitec). For production of the REST reporter gene, the canonical RE1 motif was fused to the proximal end of the thymidine kinase promoter (TK) from the pGL4.54 plasmid (Promega), using overlap extension PCR. The RE1-like sequence from the mouse *Rfx7* gene (*Rfx7*-RE1L, chr9:72,606,074-72,606,107; GRCm38/mm10 assembly) was inserted distal of the TK promoter in a synthetic gene block DNA (Integrated DNA Technologies). The RE1-TK and TK-*Rfx7*-RE1L DNA fragments were subcloned into the multiple cloning site of the promoterless firefly luciferase-encoding vector pGL4.10 (Promega) to generate the RE1-TK-pGL4.10 and TK-*Rfx7*-RE1L-pGL4.10 plasmids. The negative-control reporter gene TK-pGL4.10 was generated by subcloning the TK promoter (without an RE1) into the pGL4.10 vector. Mutant version of the TK-*Rfx7*-RE1L-pGL4.10 reporter was generated by changing the 'TCC' and 'GGT' triplets of the RE1L motif to 'TTT' in a synthetic gene block and subcloning it into pGL4.10. Human *SRRM4* and various isoforms of human *REST* were amplified by RT-PCR (see primers in Table S6) and subcloned into the pcDNA3.1+ or pLPC (Westbrook et al., 2008) expression vector.

Splicing Assays in Transfected Cells

HEK293 cells were co-transfected with the *REST* minigene (WT or DFNA27 version) and an *SRRM4*-encoding plasmid using Lipofectamine LTX and PLUS reagent (Thermo Fisher Scientific). In some experiments, the *SRRM4*-encoding plasmid was replaced with an empty pcDNA3.1+ expression vector (negative control). RNA was isolated from the cells 24 h after transfection using RNeasy Mini Kit (QIAGEN). The splicing of minigene-encoded transcripts was tested by RT-PCR (see primers in Table S6).

qRT-PCR Analysis of HDAC Inhibitor-Incubated Cells

HEK293 cells were incubated with SAHA (1 and 5 μ M), FK228 (2 and 10 nM), Merck60 (0.6 and 1.2 μ M), or DMSO (0.1%, negative control) for 36 h. During incubation with HDAC inhibitors and 0.1% DMSO, the FBS concentration in the culture medium was changed from 10% to 2% to reduce the potential binding of HDAC inhibitors to serum proteins. At the end of the 36-h incubation time, RNA was isolated using RNeasy Mini Kit (QIAGEN). The expression levels of selected REST target genes and the reference gene *G6PD* were analyzed using qRT-PCR (see primers in Table S6).

Reporter Gene-Based Assays and Immunoblotting

Neuro2a cells were transfected with the luciferase-encoding plasmids RE1-TK-pGL4.10 (firefly luciferase) and pGL4.7Rluc (renilla luciferase, 10:1 ratio of the two constructs), and expression vectors encoding the WT or DFNA27 forms of REST. Both flag-tagged and non-tagged forms of the various REST forms were tested. The presence of N-terminal flag tag did not affect the results of the assay (data not shown). In another set of experiments, Neuro2a cells were transfected with TK-*Rfx7*-RE1L-pGL4.10 and pGL4.7Rluc (10:1 ratio) or TK-*Rfx7*-RE1L^{MUT}-pGL4.10 and pGL4.7Rluc (10:1 ratio), and an expression vector encoding WT REST⁴⁻. Cells were lysed 36 h after transfection. The activities of firefly and renilla luciferases in the lysates were measured using the Dual-Luciferase Reporter Assay (Promega) and a luminometer (Wallac 1420 Multi-label Counter, PerkinElmer Life Sciences). Expression levels of WT and DFNA27 isoforms of REST were tested in transfected Neuro2a cells using immunoblotting. Cells were lysed in SDS sample buffer, boiled for 3 min, resolved by SDS-PAGE, and electroblotted onto nitrocellulose membranes. Following a blocking incubation step, monoclonal anti-flag antibody (diluted 1:1,000) or rabbit anti-LMNB1 antibody (diluted 1:5,000) was added to the membranes for 14 hours. After multiple washing steps, membranes were incubated with HRP-conjugated anti-mouse antibody (diluted 1:10,000) or HRP-conjugated anti-rabbit antibody (diluted 1:10,000). Immunoblot signals were visualized using SuperSignal West Pico Chemiluminescent Substrate (Thermo Fisher Scientific).

Incubation of Organ of Corti Cultures with HDAC Inhibitors

To analyze the effects of HDAC inhibitors on the survival of cochlear hair cell *in vitro*, organ of Corti cultures were incubated with SAHA (1 μ M), FK228 (2 nM), Merck60 (1.2 μ M), or DMSO (0.1%) from DIV2–3 to DIV9–12. SAHA was added to the cultures every 12 h because its half-life in serum is only 1–2 h (Konsoula and Jung, 2008). FK228 was added to the organ cultures once in every 3 days for 12 h; the medium was exchanged at the end of the 12-h incubation to prevent cytotoxicity associated with the prolonged presence of FK228. The Merck60-containing medium was exchanged daily because the half-life of Merck60 in aqueous solutions has not been reported. Some of the organ cultures were also treated with 5 μ M (Z)-4-hydroxytamoxifen (Tocris Bioscience) on DIV3–4 to induce Cre activity. On DIV9 or DIV12, the organ cultures were fixed with 4% PFA and labeled with phalloidin-Alexa 488 or immunostained as described in the 'Immunofluorescence and Histochemistry' section. To test the efficiency of tamoxifen-induced recombination of loxP sites *in vitro*, DNA was isolated from a subset of cultures at DIV12 using PicoPure DNA Extraction Kit (Thermo Fisher Scientific). The isolated DNA was analyzed using PCR (see primers in Table S6). To analyze FK228-dependent gene expression changes, organs of Corti were dissected from newborn mice and incubated with 2 nM FK228 or solvent only (0.1% DMSO) from DIV1 to DIV1.5 and from DIV3 to DIV3.5. RNA was isolated from these cultures at DIV3.5.

RNA Sequencing and Bioinformatics Analyses

The neocortex of 3 WT and 3 *Rest*^{+/ΔEx4} mice (E15.5) was dissected from the brain, and RNA was isolated from the dissected tissue using Trizol Reagent (Thermo Fisher Scientific). RNA was further purified on the separation column of the RNeasy Mini Kit (QIAGEN), following the manufacturer's instructions. Utricles were dissected from E15.5 WT and *Rest*^{+/ΔEx4} mice, and RNA was isolated from the dissected tissue using the RNeasy Micro Kit (QIAGEN). RNA was pooled from 7–9 mice to obtain a single sample with sufficiently high concentration for RNA-seq. In total, 25 WT mice (n = 3 samples) and 32 *Rest*^{+/ΔEx4} mice (n = 4 samples) were used for the RNA-seq experiment. The RNeasy Micro Kit (QIAGEN) was used for the isolation of RNA from organ of Corti cultures that were incubated with 2 nM FK228 or solvent. RNA was pooled from 6–8 organ of Corti cultures to obtain a single sample for RNA-seq. In total, 28 WT mice (n = 4 FK228-treated and 4 control samples) and 29 *Rest*^{+/ΔEx4} mice (n = 4 FK228-treated and 4 control samples) were used for the RNA-seq experiment. All RNA samples were processed for RNA-seq following identical protocol. 200–300 ng of total RNA were reverse transcribed using SuperScript IV reverse transcriptase (Thermo Fisher Scientific), oligo dT primer, and template switching oligo. Second strand cDNA was amplified using LongAmp DNA polymerase (New England Biolabs) for 12 PCR cycles, purified on SPRI Select Beads (Beckman Coulter), and eluted with Buffer EB (QIAGEN). The size distribution and concentration of second strand cDNA was evaluated using High Sensitivity Large Fragment Analysis Kit and a Fragment Analyzer instrument (both from Advanced Analytical). 125 pg of second strand cDNA was fragmented, PCR amplified, and indexed using the Nextera XT Library Prep Kit (Illumina). Following AMPure XP bead purification (Beckman Coulter), the size distribution and concentration of cDNA Libraries were evaluated using High Sensitivity NGS Fragment Analysis Kit (Advanced Analytical) and Fragment Analyzer. All libraries were normalized, pooled and sequenced in a HiSeq1500 instrument (126 × 126 paired end mode; Illumina). Demultiplexed samples were mapped to the mouse genome (GRCm38.p4 Release M11 from GENCODE), and transcripts were quantified using the STAR aligner (v2.5.2a) and the ‘–quantMode GeneCounts’ parameter (Dobin et al., 2013). Gene level counts were filtered to remove genes that had lower than 5 counts in all compared samples. Differential gene expression was evaluated using the DESeq2 tool (Love et al., 2014). Genes were considered differentially expressed if the adjusted p in the DESeq2 analysis was lower than 0.05. Only the RefSeq curated genes were analyzed, and pseudogenes were filtered out. The UCSC Table Browser (Karolchik et al., 2004) was used for the genome-wide analysis of REST ChIP-seq peaks from ENCODE. This ChIP-seq dataset has been generated using human cell lines (ENCODE Project Consortium, 2012). A given REST ChIP-seq peak from ENCODE was considered indicative of REST binding if the associated cluster score was higher than 850 in the ‘wgEncodeRegTfbsClusteredV2’ table of the UCSC Table Browser. Even high score peaks were filtered out if the peaks were not located within an annotated gene or maximum 6 kb upstream of the transcription start site of a gene. We refer to the mouse orthologs of these human REST-binding genes as ‘high-confidence REST targets’ (Table S2). This filtered set of REST-binding genes was considered applicable to the analysis of mouse data because the REST-binding RE1 motifs are conserved among vertebrates in 90% of the high-confidence REST target genes (Table S2). Potentially RFX-binding genes were identified in the mouse genome by searching for RFX1-binding motifs-like sequences in the ‘Hub_186875_JasparTFBS’ table using the UCSC Table Browser (Khan et al., 2018). The list of RFX1-binding motif-like sequences was filtered based on cluster score (cut-off: 400), conservation (> 0.4 mean conservation score in the ‘60-vertebrate Basewise Conservation by PhyloP’ table), and location (\pm 300 bp from a transcription start site). Potential RFX1-binding motifs that overlapped with coding regions of genes were filtered out because conservation in these regions is more likely to indicate the non-neutral evolution of a protein-coding sequence than that of a potential regulatory motif. The utricular RNA-seq data were analyzed for potential differences in alternative splicing and polyA site selection using the JunctionSeq tool (Hartley and Mullikin, 2016). Adjusted p = 0.001 was selected as cut-off for significantly different exon usage in the JunctionSeq analysis. All potential splicing differences were tested by RT-PCR (see primers in Table S6). Uniprot keyword annotations of differentially expressed genes were identified using the DAVID software (Huang da et al., 2009). All genes expressed in E16 vestibular hair cells were used as the background gene set for the Uniprot keyword annotation analysis (Scheffer et al., 2015).

SAHA Treatment of Mice

SAHA was dissolved in DMSO and diluted 2-fold in Cremophor EL (Millipore). Just before the mice were injected, the DMSO/Cremphor EL solution of SAHA was diluted further in 0.9% NaCl. *Rest*^{+/ΔEx4} and WT mice were injected subcutaneously with 100 mg SAHA/kg body weight at P2, P4 and P5. In the control group, *Rest*^{+/ΔEx4} and WT mice were injected with the vehicle solution only. At P6, the morphology of the organ of Corti and the extent of H4 acetylation were evaluated as described in the ‘Immunofluorescence and Histochemistry’ section. *Rest*^{+/ΔEx4};Rosa^{+CreERT2} mice were injected with a mixture of SAHA (100 mg/kg body weight) and (Z)-4-hydroxytamoxifen (33 mg/kg body weight) at P7, P8, and P9. From P10 to P15, the same mice were injected with SAHA only (150 mg/kg body weight/day). In the control groups, *Rest*^{+/ΔEx4};Rosa^{+CreERT2} mice were injected with (Z)-4-hydroxytamoxifen (33 mg/kg body weight/day) at P7–9 or vehicle only. WT mice were also treated with the same regimen of SAHA, (Z)-4-hydroxytamoxifen, and vehicle solution than *Rest*^{+/ΔEx4};Rosa^{+CreERT2} mice. At P16, the ABR was measured to test the hearing thresholds of mice. Subsequently, the morphology of the organ of Corti or H4 acetylation was examined as described in the ‘Immunofluorescence and Histochemistry’ section.

QUANTIFICATION AND STATISTICAL ANALYSIS

Data are presented as individual data points, mean \pm standard error of the mean (SEM), or median with minimum, maximum, 25th, and 75th percentile values, as indicated in the corresponding figure legends. The statistical methods applied are either indicated in the

figure legend or described in the main text. Sample sizes were not determined *a priori*. RNA-seq data and Uniprot keyword annotations were analyzed using the DESeq2 software and the DAVID bioinformatics tool, respectively (see ‘RNA Sequencing and Bioinformatics Analysis’ section). scQRT-PCR data were analyzed using the SINGULAR Analysis Toolset (Fluidigm) in R 3.0.2, as described in the ‘Single Cell RT-PCR’ section. All other data analyses were performed with GraphPad Prism version 7. For the datasets analyzed using GraphPad Prism, assumptions of normality were tested with the Shapiro-Wilk test and assumptions of equal variance with either the F-test (for two groups) or the Brown-Forsythe test (for three or more groups).

In cases where assumptions of normality and equal variance were not violated, parametric tests were used for the further analysis of datasets: the one-sample t test was used to compare the mean of one group to a hypothetical value; the unpaired Student’s t test was used to compare the means of two groups; and one-way or two-way ANOVA was used (depending on the number of categorical independent variables) to compare the means of three or more groups. When ANOVA revealed significant findings, the Dunnett’s post hoc test was used to compare the means of the test groups to the mean of a control group.

In the few cases where the assumption of equal variance (but not normality) was violated, Welch’s t test was used to compare the means of two groups.

In cases where the assumption of normality (but not equal variance) was violated, non-parametric tests were used for the analysis of datasets: the one-sample Wilcoxon-signed rank test was used to compare the median of one group to a hypothetical value; and the Mann-Whitney test was used to compare the medians of two groups.

In cases where assumptions of both normality and equal variance were violated, one of two approaches was selected.

- Datasets presented in Figures 4E, 4F, and the right panel of Figure S6F were log2 transformed. Analyses of these log2 transformed data with the Shapiro-Wilk test and F-test revealed that assumptions of normality (but not equal variance) were violated. Therefore, following the log2 transformation the Mann-Whitney test was used to compare the medians of two groups.
- Datasets presented in Figure 6G were analyzed using a parametric test (i.e., two-way ANOVA) without data transformation. In this figure, ceiling effects led to violations of normality and equal variance assumptions. Specifically, thresholds of 32 kHz sound-evoked ABRs were higher than the maximum tested sound pressure level (i.e., 90 dB) in two groups of Rest exon 4 deficient mice. In the context of Figure 6G, these ceiling effects increased the probability of type II error (false negative) but not the type I error (false positive).

In figure panels where multiple one-sample tests or two-group tests were used, the Benjamini-Hochberg procedure was applied to limit the false discovery rate (FDR) at 0.05, as indicated in the relevant figure legends. For gene enrichment analysis, Fisher’s exact test was used.

All reported p values are two-tailed, and p < 0.05 is considered statistically significant unless otherwise specified. Numbers of animals and biological replicates of assays (n) are reported in the figure legends if a statistical test was used or individual data points are not shown in the corresponding figure. Replicates for each experiment are outlined here:

- Figure 1C is representative of images from 3 independent assays. In each assay, one E15.5 mouse/genotype (utricle sample) and one P0 mouse/genotype (all other samples) were used. RNA was pooled from the left and right utricles of each mouse.
- Figures 1D and 1E represent data from 18 WT and 9 Rest^{+/-ΔEx4} mice.
- Figure 1F represents data from 12 WT and 10 Rest^{+/-ΔEx4} mice.
- Figures 1G and S2A are representative images of: 12 organs of Corti from 6 E17 WT mice; 8 organs of Corti from 4 P6 WT mice; 10 organs of Corti from 5 P12 WT mice; 8 organs of Corti from 4 E17 Rest^{+/-ΔEx4} mice; 10 organs of Corti from 5 P6 Rest^{+/-ΔEx4} mice; and 6 organs of Corti from 3 P12 Rest^{+/-ΔEx4} mice.
- Figure 1H is representative of images of: 6 utricles from 3 E16 WT mice; 8 utricles from 4 P6 WT mice; 10 utricles from 5 E16 Rest^{+/-ΔEx4} mice; and 14 utricles from 7 P6 Rest^{+/-ΔEx4} mice.
- Figure 1I represents data from 5 mice/group.
- Figures 1J and S3A are representative images of 10 inner ear preparations from 5 mice/group.
- Figure 2A represents data for the number of affected and unaffected subjects indicated in the LMG2 family pedigree in Figure 2B.
- Figure 3A represents data for two affected subjects from the LMG2 family and a control subject. The RT-PCR was repeated once (2 technical replicates).
- Figure 3C is representative of images from 4 independent assays.
- Figure 3G represents data from 4 independent assays.
- Figures 4A and 4B represent RNA-seq data from the number of tissue samples and mice described in the ‘RNA Sequencing and Bioinformatics Analysis’ section of Method Details.
- Figure 4D is representative of images of 14 utricles from 8 WT and 9 utricles from 6 Rest^{+/-ΔEx4} mice.
- Figures 4E and 4F represent data for 6 utricles from 3 mice/group. Individual data points represent the lengths of: 478 kinocilia in the WT E15 group; 177 kinocilia in the WT E16 group; 487 kinocilia in the Rest^{+/-ΔEx4} E15 group; 662 kinocilia in the Rest^{+/-ΔEx4} E16 group; 506 stereocilia bundles in the WT E15 group; 306 stereocilia bundles in the WT E16 group; 507 stereocilia bundles in the Rest^{+/-ΔEx4} E15 group; and 458 stereocilia bundles in the Rest^{+/-ΔEx4} E16 group.

- **Figure 5A:** Left panel is representative of images from 3 independent assays (one mouse/time point in each assay). Middle and right panels are representative of images from 2 independent assays (one sample/time point in each assay; 6–10 hearing or balance organs from 3–5 mice were pooled for each sample).
- **Figure 5C** is representative of images of 6 cortical sections from 3 mice/time point (2 cortical sections/mouse/time point).
- **Figure 5D** is representative of images of 10–12 inner ear sections from 3 mice/time point.
- **Figure 5E** represents data from 3 mice/group. 1–3 organ of Corti-containing areas were analyzed in each section. Data points indicate the intensity of EGFP signal in: 138 cortical neurons at P0; 34 cortical neurons at P16; 58 OHCs at P0; 62 OHCs at P6; 44 OHCs at P16; 23 IHCs at P0; 21 IHCs at P6; and 26 IHCs at P16.
- **Figure 5F** represents data from: 159 non-HCs isolated from 5 P1 mice; 63 non-HCs isolated from 4 P7 mice; 20 OHCs isolated from 5 P1 mice; 19 OHCs isolated from 4 P7 mice; 9 IHCs isolated from 3 P1 mice; and 4 IHCs isolated from 2 P7 mice.
- **Figures 5G and 5H** represent data from 10 non-HCs isolated from: 3 P1 mice; 10 non-HCs isolated from 3 P7 mice; 8 OHCs isolated from 3 P1 mice; 10 OHCs isolated from 3 P7 mice; 4 IHCs isolated from 3 P1 mice; and 4 IHCs isolated from 2 P7 mice.
- **Figure 6A** is representative of images of: 5 non-treated WT cultures; 4 non-treated *Rest^{+/-ΔEx4}* cultures; and 5 FK228-treated *Rest^{+/-ΔEx4}* cultures. Within a treatment group, each culture was derived from a different mouse.
- **Figure 6B** represents data from: 5 non-treated WT cultures; 4 non-treated *Rest^{+/-ΔEx4}* cultures; 5 FK228-treated *Rest^{+/-ΔEx4}* cultures; 4 SAHA-treated *Rest^{+/-ΔEx4}* cultures; and 4 Merck60-treated *Rest^{+/-ΔEx4}* cultures. Within a treatment group, each culture was derived from a different mouse.
- **Figures 6C, 6D, and S6B** represent images and data from: 4 non-treated WT mice; 4 non-treated *Rest^{+/-ΔEx4}* mice; and 6 SAHA-treated *Rest^{+/-ΔEx4}* mice. In **Figure 6D**, the hair cell counts are the average for the two ears of each mouse.
- **Figures 6E and S6D** represent data and images from 3 organ cultures/group (one organ culture/mouse/group).
- **Figures 6F and S6E** represent data and images from 3 mice/group. Hair cell counts were averaged from the two cochleas of each mouse.
- **Figure 6G** represents data from 8 mice in the '*Rest^{+/-ΔEx4}*; *Rosa^{+/CreERT2}* + T + SAHA' group and 7 mice/group in all other groups. ABR thresholds were determined for each mouse at each sound frequency indicated in the figure.
- **Figure S1B** is representative of images from 2 independent assays. DNA from 2 WT mice and 3 *Rest^{+/-NeoEx4}* mice was analyzed in these assays (one DNA sample/mouse).
- **Figure S1C** is representative of images from 3 independent assays. RNA from 3 WT and 4 *Rest^{f/fEx4/fEx4}* mice was analyzed in the 3 assays (one RNA sample/mouse were analyzed).
- **Figure S1D** represents data from 3 WT and 4 *Rest^{f/fEx4/fEx4}* mice.
- **Figure S1E** is representative of images from 3 independent assays (one mouse/genotype/assay).
- **Figure S1F** represents data from 4 mice/genotype/time point.
- **Figure S1G** is representative of images of 4 organs of Corti from 2 mice/genotype.
- **Figure S1H** is representative of images of 4 utricles from 2 mice/genotype.
- **Figure S1I** is representative of images of 8 organs of Corti and 8 utricles from 4 mice.
- **Figure S2B** is representative of images of: 6 utricles and 6 anterior cristae ampullaris from 3 E16 WT mice; 8 utricles and 8 anterior cristae ampullaris from 4 P6 WT mice; 10 utricles and 10 anterior cristae ampullaris from 5 E16 *Rest^{+/-ΔEx4}* mice; and 14 utricles and 14 anterior cristae ampullaris from 7 P6 *Rest^{+/-ΔEx4}* mice.
- **Figures S2C and S2D** represent data from the number of inner ears and mice indicated in the legend of **Figure S2**.
- **Figure S3B** is representative of images from 2 independent assays. In each assay, DNA samples from 2 WT, 3 *Rest^{+/-fEx4}*; *Rosa^{+/CreERT2}*, and 3 '*Rest^{+/-fEx4}*; *Rosa^{+/CreERT2}* + T' mice were analyzed.
- **Figure S3C** is representative of images of 6 organs of Corti of 3 mice/genotype.
- **Figure S3D** is representative of images of 4 solvent-incubated organ cultures and 5 Z-DEVD-FMK-incubated organ cultures (one culture/mouse/incubation condition).
- **Figure S3E** represents data from: 4 organ cultures incubated with solvent; 5 organ cultures incubated with Z-DEVD-FMK; and 5 organ cultures incubated with Z-VAD-FMK (one organ culture/mouse/incubation condition).
- **Figure S3F** is representative of images of 40 brain sections from 2 WT mice and 91 brain sections from 4 *Rest^{+/-ΔEx4}* mice.
- **Figure S3G** is representative of images of 16 cortical sections from 4 mice/genotype (4 sections/mouse).
- **Figure S3H** represents data from 4 mice/genotype (4 sections/mouse were analyzed).
- **Figure S3I** represents data from 3 mice/genotype (2 sections/mouse were analyzed).
- **Figure S3J** is representative of images of 61 sections from 4 WT mice and 58 sections from 4 *Rest^{+/-ΔEx4}* mice.
- **Figure S3K** represents data from: 13 WT mice at P30; 3 WT mice at P130; 4 *Rest^{+/-}* mice at P30; and 3 *Rest^{+/-}* mice at P130.
- **Figure S3M** is representative of images of 3 technical replicates/primer pair. One human RNA sample per organ was used.
- **Figure S3N** is representative of images from 2 independent assays.
- **Figure S4A** is representative of a single assay/primer pair.
- **Figure S4C** represents data from 3 mice/genotype (RNA was pooled from the left and right utricles and saccules of each mouse).
- **Figure S4G** represents data from 5 independent assays.

- [Figure S4H](#) represents data from 3 mice/genotype at each time point (RNA was pooled from the left and right utricles and saccules of each mouse).
- [Figure S4I](#) is representative of images of 4 utricles and 4 saccules from 2 ' $\text{Rest}^{+/\Delta\text{Ex4}}$, $\text{Rosa}^{+/\text{CreERT2}}$ – T' mice, and of 6 utricles and 6 saccules from 3 ' $\text{Rest}^{+/\Delta\text{Ex4}}$, $\text{Rosa}^{+/\text{CreERT2}}$ + T' mice.
- [Figure S4J](#) is representative of images of 6 utricles from 3 mice at P0 and 10 utricles from 5 mice at P16.
- [Figure S5A](#) represents data from 3 independent assays/treatment condition.
- [Figure S5B](#) is representative of images of: 5 non-treated WT cultures; 3 FK228-treated WT cultures; 3 SAHA-treated WT cultures; 3 Merck60-treated WT cultures; 4 non-treated $\text{Rest}^{+/\Delta\text{Ex4}}$ cultures; 5 FK228-treated $\text{Rest}^{+/\Delta\text{Ex4}}$ cultures; 4 SAHA-treated $\text{Rest}^{+/\Delta\text{Ex4}}$ cultures; and 4 Merck60-treated $\text{Rest}^{+/\Delta\text{Ex4}}$ cultures. Within a treatment group, each culture was derived from a different mouse.
- [Figure S5E](#) represents data from 3 independent samples/treatment condition (6–8 organ cultures from 3–4 mice were pooled to obtain a single sample).
- [Figure S6A](#) represents data from 3 organ cultures/group (one organ culture/mouse/group).
- [Figure S6C](#) is representative of images from 2 independent assays. DNA was isolated from 4 organ cultures (derived from 2 mice) to obtain a single sample. In the 2 assays, 2 samples per treatment condition were analyzed.
- [Figure S6F](#) represents data from: 36 OHCs from 2 vehicle-injected mice (left panel); 40 OHCs from 2 SAHA-injected mice (left panel); 90 OHCs from 4 vehicle-injected mice (right panel); and 48 OHCs from 4 SAHA-injected mice (right panel).

DATA AND SOFTWARE AVAILABILITY

The accession number for the RNA-seq data reported in this paper is GEO: GSE111606.

Supplemental Figures

Cell

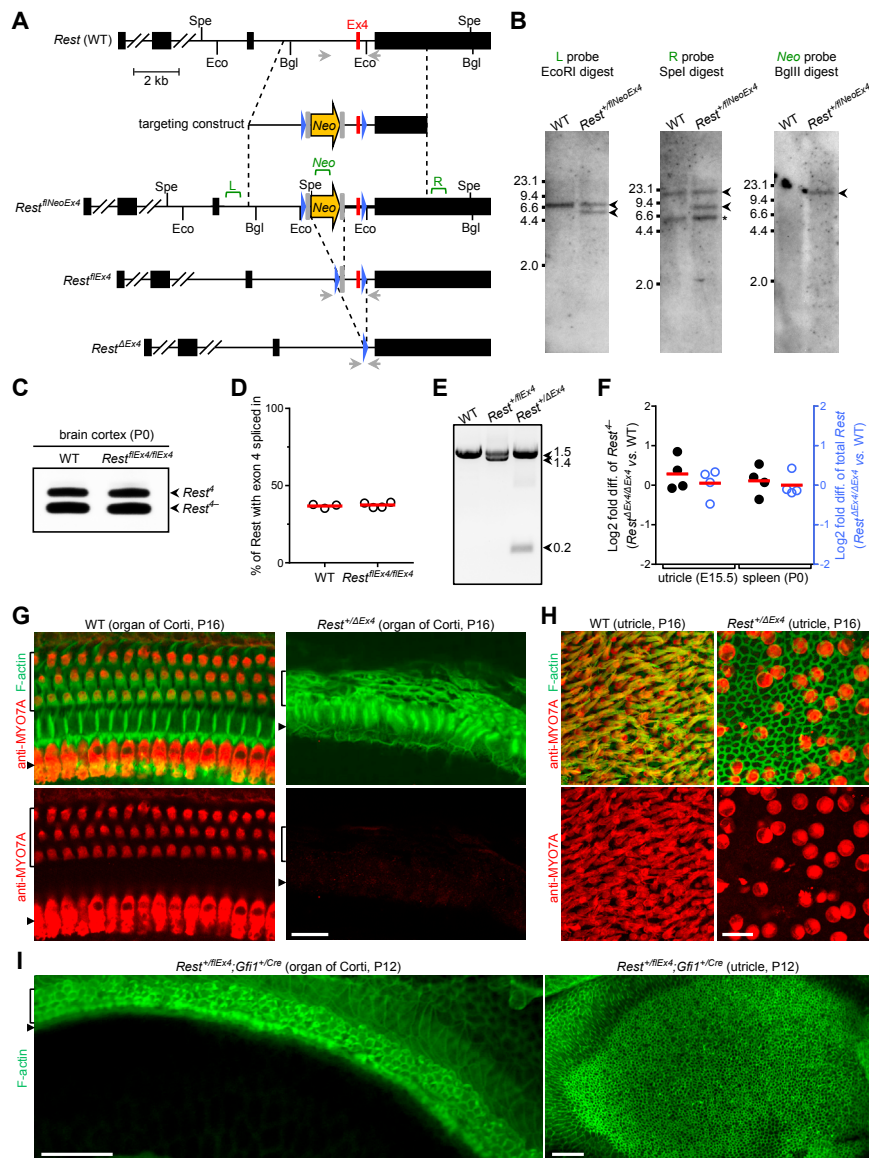


Figure S1. Genetic Deletion of Mouse Rest Exon 4 Causes Hair Cell Death in a Cell-Autonomous Manner, Related to Figure 1

(A) Strategy for conditional deletion of Rest exon 4 in mice. Schematic of WT Rest, the exon 4-targeting construct, the exon 4-floxed form of Rest that contains a neomycin resistance gene (*Rest*^{fNeoEx4}), the exon 4-floxed form of Rest that does not contain neomycin resistance gene (*Rest*^{fEx4}), and the exon 4-deleted form of Rest (*Rest*^{ΔEx4}). Dashed lines indicate regions affected by the recombination steps. Red box represents exon 4 (Ex4), and black boxes represent exons 1–3 and 5. Horizontal lines represent introns. Frt sites (gray boxes), loxP sites (blue triangles), the neomycin resistance gene (Neo, block arrow), the positions of genotyping primers (gray arrows), the locations of Spel (Spe), EcoRI (Eco) and BgIII (Bgl) restriction sites, and the positions of left (L), neomycin-resistance gene (Neo), and right (R) Southern blot probes (green brackets) are indicated.

(B) Confirmation of correct targeting of Rest exon 4 using Southern blotting. Genomic DNA from WT and *Rest*^{fNeoEx4} mice was digested with the indicated restriction enzymes and Southern blotted using the L, R, and Neo probes. Positions of the DNA size markers (short horizontal lines) and expected positions of Southern blot hybridization products (arrowheads) are indicated. Lengths of DNA size markers are shown in kilobase pairs. Asterisk indicates a non-specific hybridization product that is present in similar amounts in WT and *Rest*^{fNeoEx4} samples.

(C) RT-PCR analysis of Rest exon 4 splicing in neocortices of P0 WT and *Rest*^{fEx4/fEx4} mice.

(D) Statistical analysis of Rest exon 4 splicing in neocortices of P0 WT and *Rest*^{fEx4/fEx4} mice. Splicing was quantified as the percentage of the exon 4-containing form of Rest (*Rest*^{f+}) with respect to total Rest (all splice forms). Each symbol represents the value for an independent sample; horizontal red lines indicate means (unpaired Student's t test, $p = 0.62$).

(E) PCR analysis of genomic DNA from WT, *Rest*^{fEx4}, and *Rest*^{ΔEx4} mice using the primers shown in panel A (gray arrows). The sizes of electrophoretically separated PCR products are shown next to the gel image in kilobase pairs. The sizes of PCR products confirm that Flp- and Cre-dependent recombinations occurred in the *Rest*^{fNeoEx4} allele.

(F) qRT-PCR analysis of the *Rest*^{f+} splice form (left y axis) and a shared region of the *Rest*^{f+} and *Rest*^{f-} splice forms (right y axis) in the utricles and spleens of WT

(legend continued on next page)

and *Rest*^{ΔEx4/ΔEx4} mice at the indicated times. Each symbol represents the value for an independent sample; horizontal lines indicate means (one-sample t test, FDR-adjusted $p \geq 0.27$ for each group, hypothetical mean = 0).
(G and H) Immunofluorescence detection of the hair-cell marker MYO7A (red) and F-actin (green) in organ of Corti (G) and utricle (H) preparations from P16 WT and *Rest*^{ΔEx4/ΔEx4} mice. The expected locations of IHCs (arrowheads) and OHCs (brackets) are indicated in panel G. Scale bars, 20 μm .
(I) F-actin stained organ of Corti (left panel) and utricle (right panel) preparations from a P12 *Rest*^{ΔEx4/ΔEx4;Gfi1^{+/-Cre} mouse. The expected locations of IHCs (arrowheads) and OHCs (brackets) are indicated in the left panel. Scale bars, 50 μm .}

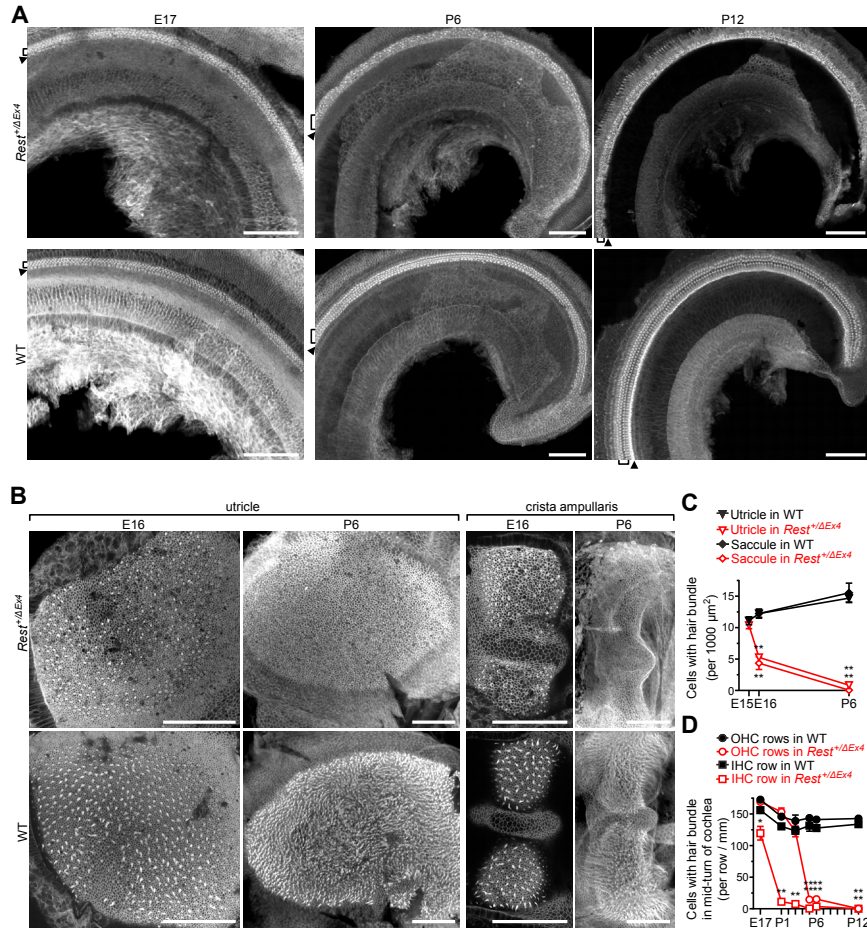


Figure S2. The *Rest*^{+/ΔEx4} Genotype Is Associated with Perinatal Degeneration of Hair Cells in the Hearing and Balance Organs, Related to Figure 1

(A and B) F-actin-stained organ of Corti (A), utricle (B), and crista ampullaris (B) from *Rest*^{+/ΔEx4} and WT mice at the indicated times. The expected locations of IHCs (arrowheads) and OHCs (brackets) are indicated in (A). Scale bars, 100 μ m.

(C and D) Statistical analysis of the numbers of cells with stereocilia bundles in the utricle (C), saccule (C), and cochlea (D) of WT and *Rest*^{+/ΔEx4} mice at the indicated times. The middle-turn region of the cochlea was analyzed. Values are mean \pm SEM ($n = 3$ mice in the following groups: WT utricle at E16, WT saccule at E16, WT saccule at P6, *Rest*^{+/ΔEx4} saccule at E16, WT OHCs at P3, WT IHCs at P5, WT OHCs at P5, *Rest*^{+/ΔEx4} OHCs at P12, and *Rest*^{+/ΔEx4} IHCs at P12; $n = 4$ mice in the following groups: WT utricle at P6, *Rest*^{+/ΔEx4} saccule at P6, WT OHCs at P6, WT IHCs at P6, *Rest*^{+/ΔEx4} OHCs at E17, *Rest*^{+/ΔEx4} IHCs at E17, *Rest*^{+/ΔEx4} OHCs at P1, *Rest*^{+/ΔEx4} IHCs at P1, *Rest*^{+/ΔEx4} OHCs at P3, *Rest*^{+/ΔEx4} IHCs at P3, *Rest*^{+/ΔEx4} OHCs at P5, and *Rest*^{+/ΔEx4} IHCs at P5; $n = 5$ mice in the following groups: WT utricle at E15, *Rest*^{+/ΔEx4} utricle at E16, WT OHCs at P1, WT IHCs at P1, WT OHCs at P12, WT IHCs at P12, *Rest*^{+/ΔEx4} OHCs at P6, and *Rest*^{+/ΔEx4} IHCs at P6; $n = 6$ mice in the following groups: *Rest*^{+/ΔEx4} utricle at E15, WT OHCs at E17 and WT IHCs at E17; $n = 7$ mice in the following group: *Rest*^{+/ΔEx4} utricle at P6). Hair cell counts from the two inner ears of each mouse were averaged for each sensory region. Welch's t test, FDR-adjusted *p = 0.038, **p < 0.0002.

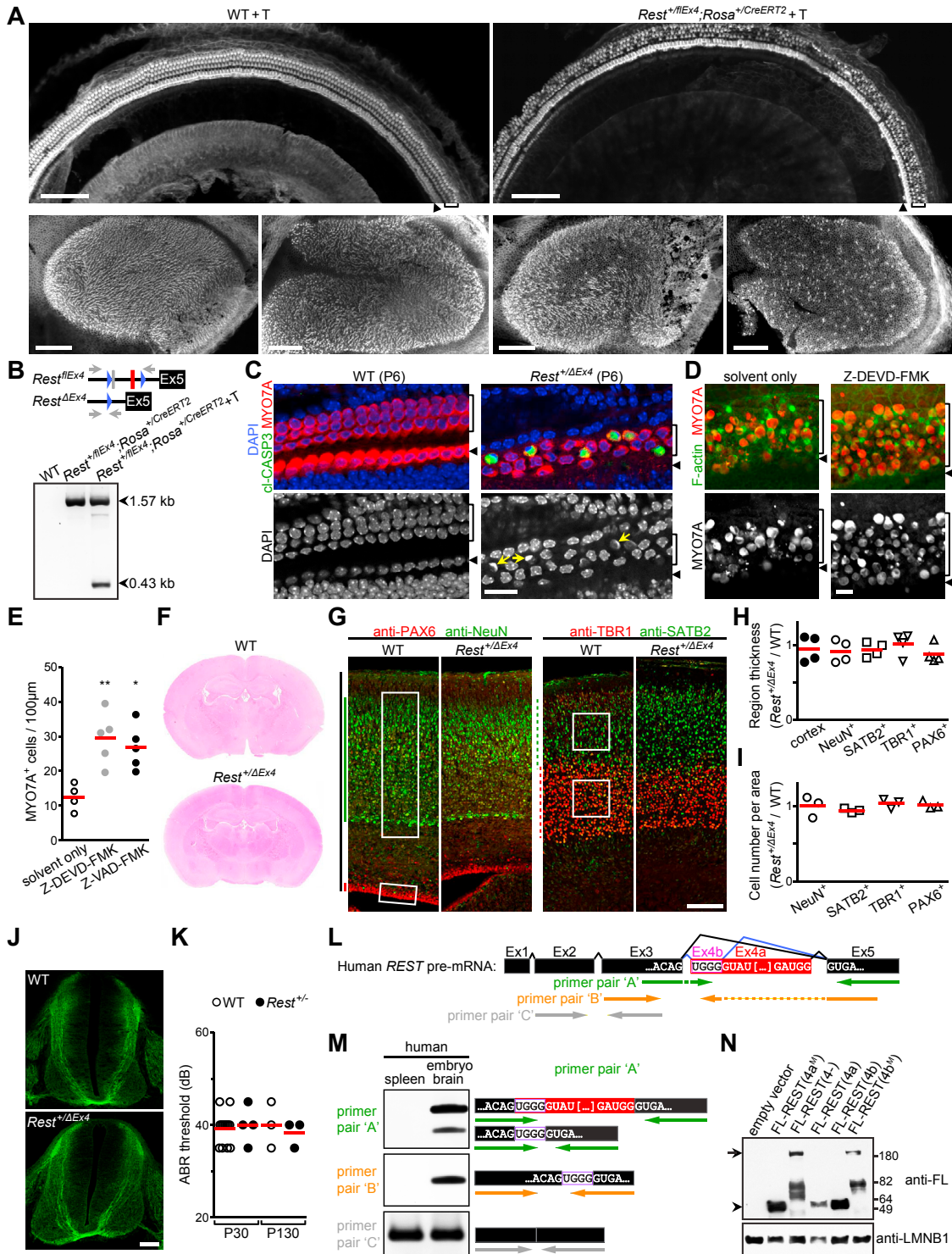


Figure S3. Exon 4 of Rest Is Critical for the Survival of Differentiated Hair Cells, but Not for Proper Layering of Neocortex or Pathfinding by Commissural Axons, Related to Figures 1 and 3

(A) Low-magnification images of F-actin-stained organ of Corti (upper panels), utricle (lower left panels), and saccule (lower right panels) from P79 WT and Rest^{+/flEx4}, Rosa^{+CreERT2} mice treated with tamoxifen (T) from P40 to P47. The locations of OHC rows (brackets) and IHC row (arrowheads) are indicated. Scale bars, 100 μm.

(B) PCR testing of tamoxifen-induced recombination of the exon 4-flanking loxP sites in Rest^{+/flEx4}, Rosa^{+CreERT2} mice. Top: Schematic of Rest^{flEx4} and Rest^{ΔEx4} alleles. Boxes represent exon 4 (red) and exon 5 (Ex5, black). Horizontal lines represent introns. LoxP sites (blue triangles), the Frt site (gray box), and the positions of

(legend continued on next page)

genotyping primers (gray arrows) are indicated. The reverse primer is complementary to the sequence of one of the loxP sites and the downstream genomic sequence. Bottom: PCR analysis of genomic DNA from the organ of Corti of a P79 WT mouse, a P79 *Rest^{+/ΔEx4};Rosa^{+/CreERT2}* mouse, and a P79 *Rest^{+/ΔEx4},Rosa^{+/CreERT2}* mouse following treatment with tamoxifen (T) from P40 to P47. The primers used in the PCR analysis are shown in the schematics at top (gray arrows). The sizes of PCR products confirm that tamoxifen-dependent recombination of loxP sites occurred in some copies of the *Rest^{+/ΔEx4}* allele. Kb, kilobase pairs.

(C) Immunofluorescence analysis of caspase-3 cleavage in the organ of Corti of a WT and a *Rest^{+/ΔEx4}* mouse at P6. Green indicates immunofluorescence signal for cleaved caspase-3 (c-CASP3); red indicates immunofluorescence signal for the hair-cell protein MYO7A. Nuclei are stained with DAPI (blue in the upper panels, white in the lower panels). Yellow arrows indicate nuclei with extensive chromatin condensation in the lower right panel. Expected locations of IHCs (arrowheads) and OHCs (brackets) are indicated. Scale bar, 20 μm.

(D) F-actin staining (green) and MYO7A immunolabeling (red) of Z-DEVD-FMK-incubated and control organ of Corti cultures derived from newborn *Rest^{+/ΔEx4}* mice. Organ cultures were exposed to Z-DEVD-FMK (100 μM) or solvent (0.5% DMSO) from day *in vitro* 2 (DIV2) to DIV9. On DIV9, cultures were fixed and stained. Expected locations of OHCs (brackets) and IHCs (arrowheads) are indicated. Scale bar, 20 μm.

(E) Statistical analysis of effects of the caspase inhibitors Z-DEVD-FMK (100 μM) and Z-VAD-FMK (100 μM) on the number of MYO7A-expressing cells in DIV9 organ of Corti cultures derived from newborn *Rest^{+/ΔEx4}* mice. Organ cultures were incubated with the caspase inhibitors or solvent from DIV2 to DIV9. Each symbol represents the value for an independent sample. Red horizontal lines indicate means (one-way ANOVA p = 0.0047, post hoc Dunnett's test *p = 0.011, **p = 0.004, control group: 'solvent only').

(F) H&E-stained brain sections from a WT and a *Rest^{+/ΔEx4}* mouse (P60).

(G) Immunostaining of sections of somatosensory cortices of a WT and a *Rest^{+/ΔEx4}* mouse (P0) with the indicated combinations of anti-PAX6, anti-NeuN, anti-TBR1 and anti-SATB2 antibodies. Vertical lines indicate the thicknesses of the entire cortex (black), the NeuN expressing layers (green), the PAX6 expressing area (red), the TBR1 expressing layers (dashed red), and the SATB2 expressing layers (dashed green). Framed regions represent cortical areas selected for cell counting in panel I. Scale bar, 100 μm.

(H) Statistical analysis of the relative thicknesses of the indicated cortical layers of P0 WT and *Rest^{+/ΔEx4}* mice. Representative images of the analyzed cortical layers are shown in panel G. n = 4 mice per genotype; four sections per mouse were analyzed. Each symbol represents averaged result for a single mouse. Horizontal red lines: means. One-sample t test, FDR-adjusted p > 0.5 for each dataset, hypothetical mean = 1.

(I) Statistical analysis of the relative densities of immunostained cells in the somatosensory cortices of P0 WT and *Rest^{+/ΔEx4}* mice. Representative areas for cell counting are shown in panel G. n = 3 mice per genotype; two sections per mouse were analyzed. Each symbol represents averaged cell count from a single mouse. Horizontal red lines: means. One-sample t test, FDR-adjusted p > 0.4 for each dataset, hypothetical mean = 1.

(J) Immunofluorescence analysis of commissural axons in transverse sections of spinal cords from WT and *Rest^{+/ΔEx4}* mice (E11.5) with an anti-TAG1 antibody. Scale bar, 100 μm.

(K) Thresholds of broadband click-evoked ABRs of WT and *Rest^{+/−}* mice at P30 and P130; each symbol represents the value for a single mouse (Mann-Whitney test, FDR-adjusted p > 0.9).

(L) Top: Schematic of the human *REST* pre-mRNA. Black rectangles represent constitutively spliced exons (Ex); purple rectangle represents exon 4b (Ex4b); red rectangle represents exon 4a (Ex4a). The sequence of exon 4b and partial sequences of exons 3, 4a, and 5 are indicated. Tented lines represent the joining of exons in the maturing pre-mRNA. Bottom: Design of RT-PCR primer pairs 'A' (green arrows), 'B' (orange arrows), and 'C' (gray arrows) used in panel M. Dashed lines indicate interruptions in the alignments of primers with the *REST* pre-mRNA at exon-exon junctions.

(M) RT-PCR analyses of alternative splicing of *REST* with primer pairs 'A' (top), 'B' (middle) and 'C' (bottom) in the indicated human tissues. Both exons 4a and 4b are absent from the *REST* mRNA in the spleen, which is used here as an example of a non-neuronal tissue. Schematic illustrations next to gel images show the exon-exon junctions revealed by the Sanger sequencing of RT-PCR products. Positions of RT-PCR primers are indicated under the scheme of the detected splice variants.

(N) Immunoblot analysis of the expression levels of flag (FL)-tagged splice forms of REST in transfected Neuro2a cells using an anti-FL antibody (upper panel). Both the physiological (4a, 4b, and 4-) and DFNA27-dependent splice forms (4a^M and 4b^M) were tested, as indicated. Negative control Neuro2a cells were transfected with an empty expression vector. Positions of the 49, 64, 82, and 180 kDa standards (short horizontal lines) and the expected positions of REST^{4−} (arrow) and REST^{4a} (arrowhead) are indicated. Loading is comparable, as evident from the similarity in the Lamin-B1 (LMNB1) signal across the samples (lower panel).

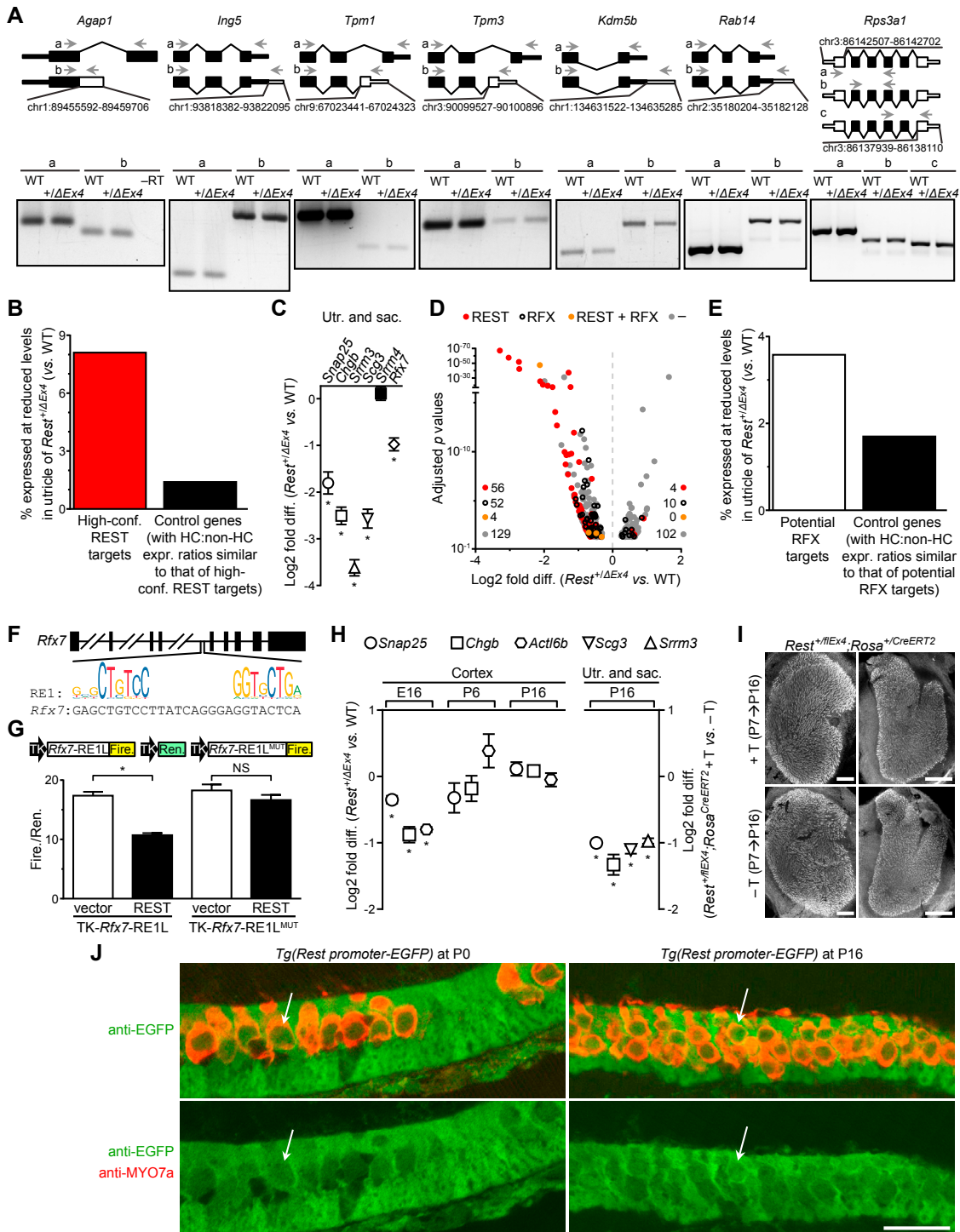


Figure S4. The Lack of Alternative Splicing-Dependent Inactivation of REST Is Not Compensated for by Transcriptional Silencing in the Ear, Related to Figures 4 and 5

(A) RT-PCR testing of potential defects in alternative splicing and polyadenylation (poly[A]) site selection as revealed by the RNA-seq analyses of the utricles of *Rest*^{+/ΔEx4} and WT mice at E15.5. Top: Schematics of the tested exons and poly(A) sites in the indicated mRNAs. Thick black rectangles represent constitutively spliced exons; tented lines represent the joining of exons in maturing pre-mRNAs. Open boxes represent exons that are candidates for differential splicing or differential poly(A) site selection; the genomic position of each of these exons is indicated (GRCm38/mm10 genome assembly). The UTRs (thinner rectangles), the positions of RT-PCR primers (gray arrows), and the names of primer pairs (lower case letters) are indicated. Bottom: RT-PCR products generated from the

(legend continued on next page)

utricle mRNAs of *Rest^{+/-Ex4}* and WT mice (E15.5) using the indicated primer pairs. This analysis did not validate the potential differences in splicing and poly(A) site selection. ‘–RT’ indicates the minus reverse transcription control in the *Agap1* panel.

(B) Percentages of high-confidence REST target genes and control genes expressed at lower levels in the utricle of *Rest^{+/-Ex4}* mice than in that of WT mice at E15.5 (Fisher’s exact test $p < 0.0001$). Control genes were selected in a two-step process: all genes were ranked based on their expression ratios in utricular hair cell versus non-hair cells (Scheffer et al., 2015), and the two direct neighbors of each high-confidence REST target were selected from the ranked list.

(C) qRT-PCR analysis of the expression of five high-confidence REST targets (*Snap25*, *Chgb*, *Srrm3*, *Scg3*, and *Srrm4*) and *Rfx7* in the vestibular system (utricle and saccule regions) of *Rest^{+/-Ex4}* versus WT mice at E16. Values are mean \pm SEM ($n = 3$ mice; one-sample t test, FDR-adjusted * $p < 0.05$, theoretical mean = 0).

(D) Volcano plot of significant differences in gene expression between the utricles of E15.5 *Rest^{+/-Ex4}* and WT mice. Red dots indicate high-confidence REST targets (REST). Open black circles indicate genes containing RFX-binding motif-like sequences in conserved regions near transcription start sites (RFX). Orange dots indicate high-confidence REST targets that also contain RFX-binding motif-like sequences in conserved regions near transcription start sites (REST + RFX). Gray dots represent genes that do not fit into the first 3 groups (–). The number of genes in each group is indicated on the left or right side of the plot depending on the direction of the defect in gene expression in *Rest^{+/-Ex4}* mice.

(E) Percentage of potential RFX target genes and control genes expressed at lower levels in the utricle of *Rest^{+/-Ex4}* mice than in that of WT mice at E15.5 (Fisher’s exact test $p = 0.0006$). Potential RFX target genes were defined as genes containing RFX-binding motif-like sequences in conserved regions near transcription start sites. Control genes were selected in a two-step process: all genes were ranked based on their expression ratios in utricular hair cell versus non-hair cells (Scheffer et al., 2015), and the two direct neighbors of each potential RFX target gene were selected from the ranked list.

(F) Top: Diagram of the exon-intron structure of mouse *Rfx7*. Rectangles represent exons; horizontal lines represent introns. Bottom: An RE1-like sequence from *Rfx7* aligned with the sequence logo of the RE1 motif.

(G) Effect of the RE1-like sequence from mouse *Rfx7* (*Rfx7-RE1L*) on the expression of a reporter gene in Neuro2a cells that were transfected with REST or an empty vector. Illustration at top shows the composition of the reporter gene (left), the control construct (middle), and the mutant (MUT) version of the reporter gene (right) in which the ‘TCC’ and ‘GGT’ sequences of the RE1-like motif were changed to ‘TTT’. Values are mean \pm SEM ($n = 5$ for each construct; unpaired Student’s t test, FDR-adjusted * $p < 0.0001$, $p = 0.13$ [not significant, NS]).

(H) Left: qRT-PCR analysis of expression levels of the indicated high-confidence REST target genes in the neocortex of *Rest^{+/-Ex4}* versus WT mice at the indicated times. Right: qRT-PCR analysis of expression levels of the indicated high-confidence REST targets in the vestibular system (utricle and saccule regions) of tamoxifen-injected (+ T) versus vehicle-injected (– T) *Rest^{+/-Ex4}; Rosa^{+/CreERT2}* mice at P16. Tamoxifen or vehicle solution was injected at P7, P8, and P9. Values are mean \pm SEM ($n = 3$ mice; one-sample t test, FDR-adjusted * $p < 0.05$, theoretical mean = 0).

(I) Low-magnification images of F-actin-stained utricle (left) and saccule (right) preparations from P16 *Rest^{+/-Ex4}; Rosa^{+/CreERT2}* mice injected with tamoxifen (+ T) or vehicle (– T) at P7, P8, and P9. In these regions of the inner ear, hair-cell degeneration was not detected 9 days after tamoxifen injection. Scale bars, 100 μ m.

(J) Immunofluorescence detection of EGFP (green) and MYO7A (red) in utricular sections from *Tg(Rest promoter-EGFP)* mice at P0 and P16. Arrows point to the same hair cells in the upper and lower panels. Scale bar, 20 μ m.

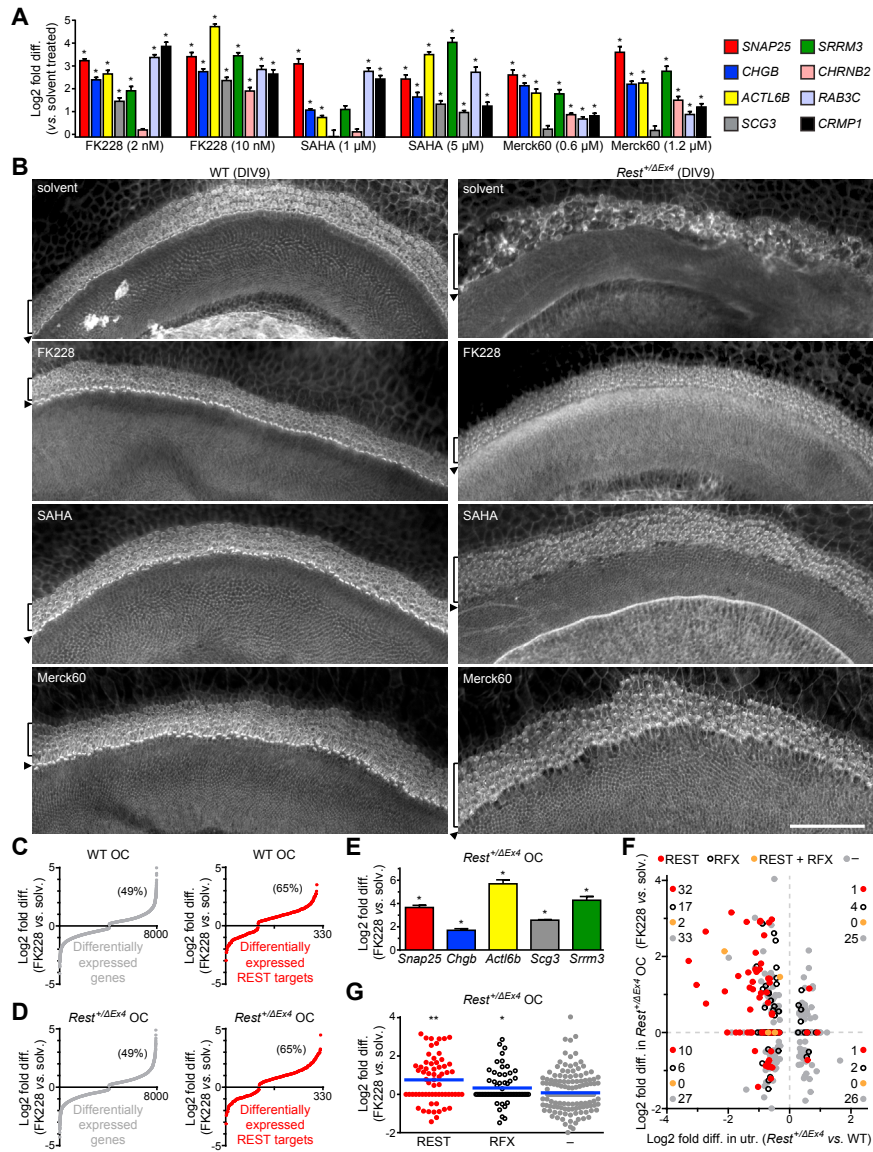


Figure S5. HDAC Inhibitors Increase the Expression of Many REST Targets and Rescue the OHCs of Rest^{+/-ΔEx4} Mice in Organ Cultures, Related to Figure 6

(A) Effects of three HDAC inhibitors (FK228, SAHA, and Merck60) on the expression levels of indicated REST target genes in HEK293 cells. Cells were incubated with the indicated concentrations of HDAC inhibitors or solvent for 36 h. Gene expression was measured using qRT-PCR. Values are mean ± SEM ($n = 3$; one-sample t test, FDR-adjusted * $p < 0.05$, theoretical mean = 0).

(B) F-actin staining of DIV9 organ of Corti cultures derived from P1 WT and Rest^{+/-ΔEx4} mice. The organs were incubated with FK228 (2 nM), SAHA (1 μM), Merck60 (1.2 μM), or solvent from DIV2 to DIV8. The expected locations of OHCs rows (brackets) and the IHC row (arrowheads) are indicated. Scale bar, 100 μm.

(C and D) FK228-dependent changes in gene expression in DIV3.5 organ of Corti (OC) cultures derived from newborn WT (C) and Rest^{+/-ΔEx4} mice (D). Organ cultures were exposed to FK228 (2 nM) or solvent twice (DIV1-1.5 and DIV3-3.5). Left panels: FK228-induced changes in gene expression. Right panels: FK228-induced changes in the expression of high-confidence REST targets. Numbers in parentheses indicate the percentage of differentially expressed genes that are upregulated by FK228. The names of differentially expressed genes are shown in Table S5.

(E) Effect of FK228 on expression of indicated high-confidence REST targets in DIV3.5 organ of Corti (OC) cultures derived from newborn Rest^{+/-ΔEx4} mice. Expression levels were measured using qRT-PCR. Values are mean ± SEM ($n = 3$ per treatment group; one-sample t test, FDR-adjusted * $p < 0.05$, theoretical mean = 0).

(F) FK228-induced changes in gene expression in DIV3.5 organ of Corti (OC) cultures derived from newborn Rest^{+/-ΔEx4} mice (y axis), plotted against differences in gene expression in the utricles of Rest^{+/-ΔEx4} versus WT mice (x axis). Expression levels were determined using RNA-seq and plotted only for the genes that are significantly up- or downregulated in the utricles of Rest^{+/-ΔEx4} mice. Red dots indicate high-confidence REST targets (REST). Open black circles indicate genes that contain RFX-binding motif-like sequences in conserved regions near transcription start sites (RFX). Orange dots indicate high-confidence REST targets that also contain RFX-binding motif-like sequences in conserved regions near transcription start sites (REST + RFX). Gray dots represent genes that do not fit into the

(legend continued on next page)

first 3 groups (-). The number of genes in each group is indicated in the plot.
(G) Statistical analysis of FK228-dependent changes in gene expression in DIV3.5 organ of Corti (OC) cultures derived from newborn *Rest^{+/ΔEx4}* mice. Expression levels were determined using RNA-seq and plotted only for the genes that are significantly up- or downregulated in the utricles of *Rest^{+/ΔEx4}* mice. Color coding of gene groups is as in (F). Blue horizontal lines indicate the means (one-sample Wilcoxon signed-rank test, FDR-adjusted *p = 0.0038, **p < 0.0003, theoretical mean = 0).

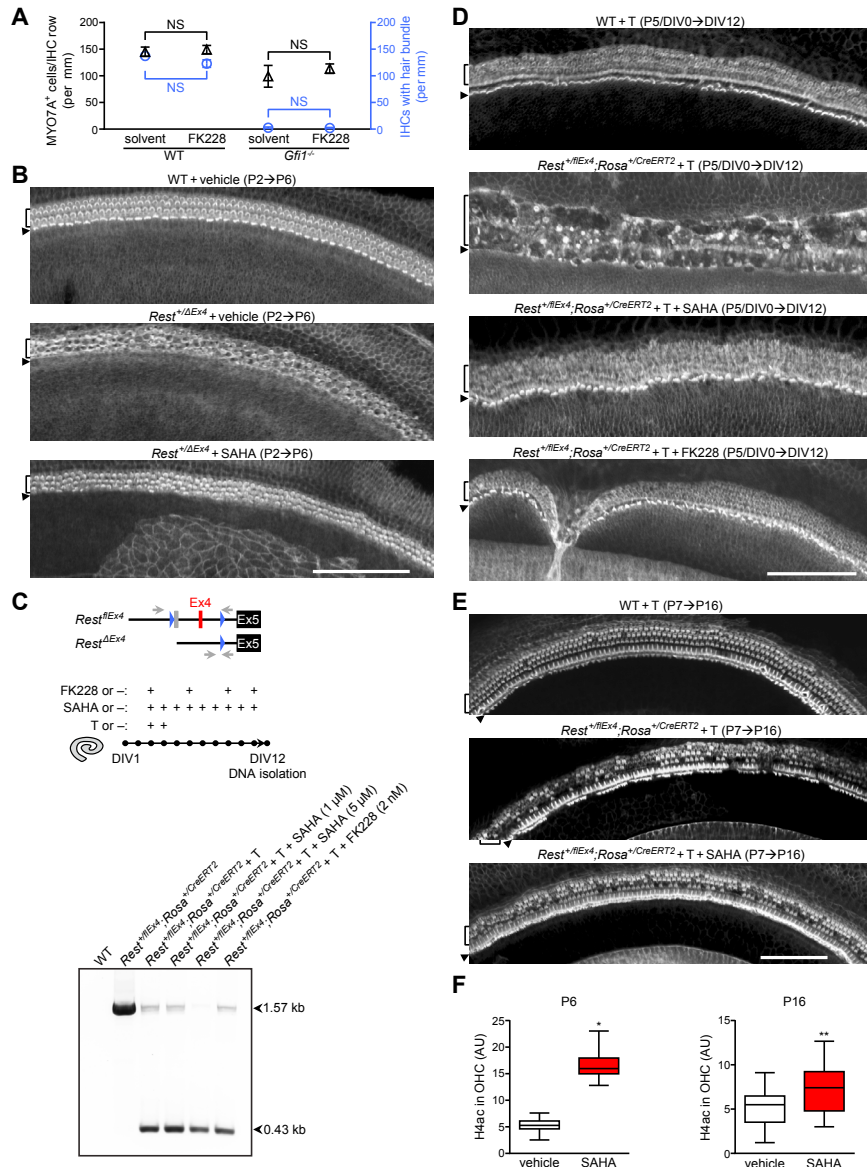


Figure S6. HDAC Inhibitors Can Rescue Both the Inner and OHCs of Rest Exon 4 Heterozygous Knockout Mice, Related to Figure 6

(A) Quantitation of the number of cells with stereocilia bundles and MYO7A immunolabeling in organ of Corti cultures derived from newborn WT and *Gfi1*^{-/-} mice. The organ cultures were incubated with FK228 (2 nM) or solvent from DIV2 to DIV8 and stained on DIV9 (as shown in Figure 6A). Reduction in the number of F-actin stained stereocilia bundles in the row of IHCs was used as an indicator of hair-cell degeneration. Reduction in the number of MYO7A-positive cells in the IHC row was used as an indicator of hair cell death. Values are mean ± SEM ($n = 3$ cultures in each group [1 culture/group/mouse]; unpaired Student's t test, FDR-adjusted $p \geq 0.45$ [not significant, NS]).

(B) F-actin staining of organ of Corti from P6 WT and *Rest*^{+/-Ex4} mice that were injected with SAHA or vehicle on P2, P4, and P5 (see protocol in Figure 6C). The expected locations of IHCs (arrowheads) and OHCs (brackets) are indicated. Scale bar, 100 μm.

(C) PCR testing of the effects of SAHA and FK228 on the efficacy of tamoxifen-induced recombination of loxP sites in organ of Corti cultures from *Rest*^{+/-Ex4}; *Rosa*^{+/-CreERT2} mice. Top: schematics of the *Rest*^{+/-Ex4} and *Rest*^{-/-Ex4} alleles. Boxes represent exon 4 (Ex4, red) and exon 5 (Ex5, black). Horizontal lines represent introns. LoxP sites (blue triangles), the Frt site (gray box), and the positions of genotyping primers (gray arrows) are indicated. The reverse primer is complementary to the sequence of one of the loxP sites and the downstream genomic sequence. Middle: schematic diagram of the durations of incubations of organ of Corti cultures with tamoxifen (T), SAHA (1 and 5 μM), FK228 (2 nM), or solvent. Bottom: PCR testing of organ of Corti cultures for the recombination of loxP sites using the PCR primers shown in the schematics at top (gray arrows). The sizes of PCR products confirm that tamoxifen-dependent recombination of loxP sites occurred. Kb, kilobase pairs.

(D) F-actin staining of DIV12 organ of Corti cultures derived from P5 WT and *Rest*^{+/-Ex4}; *Rosa*^{+/-CreERT2} mice. Tamoxifen (T) was added to cultures in the indicated combinations with SAHA (1 μM) and FK228 (2 nM). The incubation schedule is shown in (C). The expected locations of IHCs (arrowheads) and OHCs (brackets) are indicated. Scale bar, 100 μm.

(legend continued on next page)

(E) F-actin stained organ of Corti preparations from P16 WT and *Rest^{+/-}IEEX4; Rosa^{+/-CreERT2}* mice that were treated with the indicated combinations of tamoxifen (T) and SAHA or vehicle from P7 to P15 (see treatment protocol in [Figure 6F](#)). Scale bar, 100 μ m.

(F) Statistical analysis of histone H4 acetylation (H4ac) in the OHCs of SAHA- and vehicle-injected WT mice at P6 (left) and P16 (right). SAHA or vehicle was injected into mice three times (P6 group) or nine times (P16 group) as shown in [Figures 6C](#) and [6F](#). The extent of H4ac was determined based on the intensity of H4ac immunostaining. Boxplots show the maximum and minimum values in each group (whiskers), the 25th and 75th percentiles (lower and upper borders of boxes), and the median (horizontal lines in the middle of boxes). n = 36 OHCs of 2 vehicle-injected P6 mice; 40 OHCs of 2 SAHA-injected P6 mice; 90 OHCs of 4 vehicle-injected P16 mice; and 48 OHCs of 4 SAHA-injected P16 mice. Welch's t test *p < 0.0001 (left panel); Mann-Whitney test **p < 0.0001 (right panel).